Contents lists available at SciOpen

Food Science and Human Wellness

journal homepage: https://www.sciopen.com/journal/2097-0765

China Food Publishing Co.

Polygonatum sibiricum polysaccharides attenuated colitis via regulating gut microbiota mediated colonic NLRP3/ASC/Caspase-1/GSDMD signaling pathway

Zhongyu Yuan[a], Xinyu Wang[a], Jun Wang[a], Yuan Xu[a], Jing Chen[a], Shuqi Yu[a], Zhiming Chen[a], Peilu Chen[b], Jixiao Zhu[c], Weifeng Huang[d,*], Guanghui Xu[b,*], Litao Yi[a,e,f,*]

[a] *Department of Chemical and Pharmaceutical Engineering, College of Chemical Engineering, Huaqiao University, Xiamen 361021, China*
[b] *Xiamen Medicine Research Institute, Xiamen 361008, China*
[c] *Research Center of Traditional Chinese Medicine Resources and Ethnic Medicine, Jiangxi University of Chinese Medicine, Nanchang 330004, China*
[d] *Department of Gastroenterology and Hepatology, The First Affiliated Hospital of Xiamen University, School of Medicine, Xiamen University, Xiamen 361003, China*
[e] *Institute of Pharmaceutical Engineering, Huaqiao University, Xiamen 361021, China*
[f] *Fujian Provincial Key Laboratory of Biochemical Technology, Huaqiao University, Xiamen 361021, China*

ARTICLE INFO

Article history:
Received 27 February 2024
Received in revised form 16 March 2024
Accepted 24 April 2024

Keywords:
Polygonatum sibiricum
Colitis
Inflammation
NOD-like receptor protein 3
Gut microbiota
Intestinal barrier

ABSTRACT

Polygonatum sibiricum has long been a popular functional food in Asia, known for its anti-inflammatory properties. However, its efficacy in alleviating colitis has yet to be investigated. This study aimed to explore the therapeutic potential of *P. sibiricum* polysaccharides (PSP) in dextran sulfate sodium (DSS)-induced colitis, focusing on the related pyroptosis mechanisms. Scanning electron microscopy (SEM) analysis showed that PSP possesses a smooth surface with no pore structure and a dense, lamellar structure adorned with numerous spherical entities. PSP treatment significantly reduced colitis symptoms and decreased pro-inflammatory cytokines, likely through suppression of the Toll like receptor 4 (TLR4)/nuclear factor κB (NF-κB) signaling pathway. Additionally, PSP attenuated NOD-like receptor protein 3 (NLRP3)/apoptosis-associated speck-like protein containing a CARD (ASC)/Caspase-1/Gasdermin D (GSDMD)-mediated pyroptosis and mitochondria damage in the colon, while enhanced the expression of tight junction and adherens junction proteins. Microbiota sequencing showed that PSP increased the abundance of phylum Bacteroidota and genus such as g_unclassified_f_Muribaculaceae, *Lactobacillus*, Clostridia_UCG-014, and Lachnospiraceae_NK4A136_group, while decreased the phylum Proteobacteria and the genus *Enterobacter*, *Escherichia-Shigella*, and *Blautia*. In conclusion, this study demonstrates that PSP exerts the potential therapeutic role against colitis, which was mediated by the regulation of gut microbiota and the inhibition of colonic NLRP3/ASC/Caspase-1/GSDMD signaling pathway.

© 2025 Beijing Academy of Food Sciences. Publishing services by Tsinghua University Press.
This is an open access article under the CC BY-NC-ND license
(http://creativecommons.org/licenses/by-nc-nd/4.0/).

1. Introduction

Colitis, a digestive system disorder characterized by gut inflammation, can result from various causes, including viral or bacterial infections, allergies, immune system reactions, and environmental factors[1-2]. Colitis significantly impacts human health, presenting symptoms like abdominal pain, diarrhea, bloody stools, anemia, weight loss, and fever[3]. It can lead to severe complications such as colon cancer, malnutrition, and intestinal strictures. However, the pathogenesis of colitis is not fully understood and is thought to involve disrupted intestinal mucosal barriers, the release of inflammatory mediators, gut microbiota dysbiosis, abnormal immune responses, environmental influences, and autoimmunity.

Pyroptosis is one of programmed cell death characterized by the release of pro-inflammatory cellular contents[4]. The pyroptosis in

* Corresponding authors.
E-mail address: hwf0625@xmu.edu.cn (W.F. Huang); xghcxm@163.com (G.H. Xu); litaoyi@hqu.edu.cn (L.T. Yi)
Peer review under responsibility of Beijing Academy of Food Sciences.

SciOpen Publishing services by Tsinghua University Press

http://doi.org/10.26599/FSHW.2024.9250291
2213-4530/©2025 Beijing Academy of Food Sciences. Publishing services by Tsinghua University Press. This is an open access article under the CC BY-NC-ND license (http://creativecommons.org/licenses/by-nc-nd/4.0/).

colitis is closely associated with the NOD-like receptor protein 3 (NLRP3)/apoptosis-associated speck-like protein containing a CARD (ASC)/Caspase-1/Gasdermin D (GSDMD) signaling pathway[5]. Cellular stress or damage triggers the activation of the NLRP3 inflammasome, which then recruits the adaptor protein ASC, leading to the activation of caspase-1 and subsequent cleavage of GSDMD. The N-terminal fragment of GSDMD forms pores in the cell membrane, resulting in cell lysis and the release of inflammatory cytokines[6]. In colitis, uncontrolled activation of this pathway exacerbates tissue damage, causes inflammatory responses, and compromises the integrity of the colonic mucosal barrier[7]. Therefore, a detailed understanding of the NLRP3/ASC/Caspase-1/GSDMD-mediated pyroptosis is crucial for unraveling molecular basis of colitis and identifying therapeutic targets.

Polygonatum sibiricum, a widely recognized functional herbal food from the *Polygonatum* genus in the Liliaceae family, is rich in various chemical components such as polysaccharides, saponins, alkaloids, polyphenols, flavonoids, and sulfides[8-9]. Its primary active component, *P. sibiricum* polysaccharides (PSP), has been identified to offer significant pharmacological advantages[10]. PSP can modulate immune system functions, enhance immune cell activation, and strengthen immunity[11]. PSP has also been found to inhibit the Toll like receptor 4 (TLR4)/nuclear factor κB (NF-κB) signaling pathway in different animal models, including those for metabolic hypertension, depression, and lung injury[12-14]. Considering the role of TLR4/NF-κB signaling pathway-related inflammation in colitis pathophysiology and the potential of PSP to inhibit this pathway, we hypothesize that PSP could possess therapeutic effects against colitis by modulating inflammation-driven pyroptosis. In this respect, this study aimed to assess the structural characteristics of PSP and explore its impact on dextran sulfate sodium (DSS)-induced colitis in mice. Additionally, the study aimed to elucidate the therapeutic mechanism of PSP, particularly through its influence on NLRP3/ASC/Caspase-1/GSDMD-mediated pyroptosis and the gut microbiota in mice.

2. Materials and methods

2.1 Animals

Eight-week-old male ICR mice, with an average weight of (25 ± 1) g, were provided by Slac Animal Center in Shanghai, China. Upon their arrival at the laboratory, these mice were housed under temperature of (22 ± 2) ℃ and relative humidity of (55 ± 5)%. Throughout the experiment, the mice had *ad libitum* access to water and standard rodent chow. To minimize stress and ensure they were well-adapted to the new environment and human interactions, the mice underwent a one-week acclimatization and handling phase. All experiments with the utmost regard for ethical considerations and animal welfare were approved by the Experimental Animal Management Committee of Huaqiao University (approval No. A2022043, on 07/08/2022). Furthermore, all procedures were in strict adherence to the committee's guidelines and regulations for the care and management of experimental animals.

2.2 Chemical reagents

DSS (D808272, molecular weight 40 000 Da) was purchased from Maclin (Shanghai, China). Interleukin 1β (IL-1β, ab254360), IL-6 (ab9324), tumor necrosis factor α (TNF-α, ab183218), NLRP3 (ab270449), p-NF-κB (ab86299), CD68 (ab53444), inducible nitric oxide synthase (iNOS) (ab283655), zonula occludens-1(ZO-1) (ab221547 for immunofluorescence), occludin (ab216327), claudin-1 (ab307692), donkey anti-rat IgG H + L (Alexa Fluor® 568) preadsorbed (ab175475), donkey anti-rabbit IgG H + L (Alexa Fluor® 488) preadsorbed (ab150061), donkey anti-rabbit IgG H + L (Alexa Fluor® 647) preadsorbed (ab150067) and donkey anti-mouse IgG H + L (Alexa Fluor® 647) preadsorbed (ab150111) antibodies were purchased from Abcam (Cambridge, USA). GSDMD-N (PA5-116815 for Western blot) was purchased from Thermo Fisher Scientific (Waltham, USA). TLR4 (66350-1-Ig), ASC (10500-1-AP), GSDMD-N (66387-1-Ig for immunofluorescence), and ZO-1 (21773-1-AP for Western blot) were purchased from Proteintech (Wuhan, China). Caspase-1 (ES7678) was purchased from ELK Biotechnology (Wuhan, China). *β*-Actin (AC043) was purchased from ABclonal (Wuhan, China). E-cadherin (3195) was purchased from Cell Signaling Technology (Danvers, USA).

2.3 Extraction of PSP

P. sibiricum was collected from Lueyang district (Hanzhong, China), and authenticated as *P. sibiricum* Red by Cheng-Fu Li from Xiamen Hospital, affiliated to Dongzhimen Hospital, Beijing University of Traditional Chinese Medicine. The material was then defatted by refluxing with petroleum ether in a 1:5 weight-to-volume ratio at 50 ℃ for 1 h. After refluxing, the mixture was filtered, and the residue was extracted with 85% ethanol (in a 1:5 weight-to-volume ratio) for 12 h. The extract was centrifuged at 3 000 × *g* for 10 min, and the precipitates were collected, followed by ethanol evaporation under reduced pressure to obtain a pre-treated sample powder. This powder was subjected to aqueous extraction in 15-fold distilled water, stirred at 80 ℃ for 2 h. Post-extraction, the supernatant was decanted after centrifugation, with the extraction repeated twice more. The combined supernatants were concentrated to about a quarter of their original volume, and anhydrous ethanol was added to reach 80% final concentration. Following overnight incubation, the precipitates were centrifuged at 4 800 × *g* for 10 min, redissolved in a water bath at 80 ℃, and then the residual ethanol was removed under vacuum. Protein removal was conducted using the Sevag method (4:1 (*V*/*V*) chloroform to *n*-butanol). The solution was then vacuum-concentrated, placed in a dialysis bag (6 000 Da molecular weight cutoff), and dialyzed in distilled water for 48 h. The final purified product was concentrated and freeze-dried to yield the purified polysaccharide of PSP.

2.4 Characterization of PSP

Molecular weight determination by high-performance gel permeation chromatography (HPGPC) involved dissolving the polysaccharides in $NaNO_3$ solution and conducting analyses using a MIXED column (Agilent PL Aquagel-OH MIXED 8-μm column). The chromatographic settings were as follows: column temperature 35 ℃, mobile phase 0.1 mol/L $NaNO_3$, flow rate 1.0 mL/min. A refractive index detector (RID) was used, set at 40 ℃, with a sample injection volume of 4 μL. The molecular weight of PSP, as determined by HPGPC, was 1.95×10^4 Da.

For scanning electron microscopy (SEM), PSP powder was mounted on double-sided adhesive tape and sputter-coated with gold to enhance conductivity. SEM imaging was conducted at an accelerating voltage of 3.00 kV, with magnifications of 500× and 5 000×.

In Fourier transform infrared (FTIR) spectroscopy, PSP powder was mixed with anhydrous KBr, thoroughly ground, and pressed into a pellet. Infrared spectra were obtained by scanning within the wavenumber range of 4 000–500 cm^{-1}.

Nuclear magnetic resonance (NMR) analysis was performed by dissolving PSP powder in deuterated dimethyl sulfoxide (DMSO). Both ^{1}H NMR and ^{13}C NMR spectra were acquired at 25 °C on a Bruker Avance 500 spectrometer, with data processing conducted using MestNova software.

2.5 Establishment of colitis and drug treatment

Initially, the mice were randomly allocated into 4 groups (7 per group): Normal-vehicle, Colitis-vehicle, Normal-PSP, and Colitis-PSP. Firstly, 3% DSS aqueous solution was prepared by dissolving DSS in distilled water, while PSP was dissolved to a concentration of 300 mg/10 mL (equivalent to 300 mg/kg). During the first week, all groups received distilled water, and from the second week onwards, the DSS solution was administered to induce colitis. The Normal-vehicle and Normal-PSP groups continued to receive distilled water throughout the study, whereas the Colitis-vehicle and Colitis-PSP groups were given the DSS solution starting from the second week. PSP was orally administered to the designated mice at 300 mg/kg daily for 14 days (7 days before and during the DSS treatment) using gavage at 10 mL/kg. The PSP dosage was determined based on previous research and our preliminary experiment[15]. Briefly, the dose of PSP (300 mg/kg) was selected based on our small sample preliminary experiment, which contained a group of positive control 5-aminosalicylic acid (5-ASA). In the present study, the choice not to include a positive control was strategic, aimed at initially isolating the specific effects of PSP in colitis induction and treatment. The two-way ANOVA (four groups, 2 × 2) was used to evaluate the independent and combined effects of PSP and DSS treatments.

2.6 Disease activity index (DAI) analysis

Throughout the study, mice were monitored daily. DAI was evaluated daily for each mouse, based on three main parameters, each with a specific scoring system outlined in Table 1. Following euthanasia, a midline abdominal incision was performed, and the entire colon was meticulously removed. It was then carefully cleared of any attached fat or connective tissue, straightened, and measured from the cecum to the rectum using a calibrated ruler.

Table 1
Scoring criteria for DAI.

Fecal viscosity	Blood in the stool	Percentage of weight loss (%)	Score
Normalcy	No blood in stool	< 1	0
Soft stool	Minor blood in stool	1–5	1
Diarrhea stool	Frequent bloody stools	5–10	2
Watery stool	Severe bloody stool	> 10	3

2.7 Histopathological evaluation

Colonic tissues were collected and fixed in 4% paraformaldehyde for 24 h. After fixation, the tissues were processed and embedded in paraffin, and then sectioned at a thickness of 5 μm using a microtome. The sections were deparaffinized with xylene and rehydrated through a graded ethanol series to distilled water. For hematoxylin and eosin (H&E) staining, sections were stained with Harris hematoxylin solution for 5 min, rinsed in tap water, and differentiated in 1% acid alcohol for a few seconds. They were then rinsed, turned blue in 0.2% ammonia water for 30 s to 1 min, and rinsed again before being counterstained with eosin for 2 min. After dehydration in graded ethanol, sections were cleared in xylene and mounted with resinous medium.

For periodic acid-Schiff (PAS) staining, sections were oxidized in 0.5% periodic acid for 10 min, rinsed thoroughly, and incubated in Schiff's reagent for 15 min. Following another water rinse for 10 min to develop the magenta color, they were dehydrated, cleared in xylene, and mounted in resinous medium.

Both H&E and PAS stained sections were examined under a light microscope to assess general morphology and specific structures. The histopathological score was determined by evaluating three criteria: infiltration of inflammatory cells, reduction of goblet cells, and integrity of crypt structure, as detailed in Table 2.

2.8 Immunofluorescence analysis

Colonic tissues were harvested, rinsed with phosphate buffered saline (PBS), and fixed in 4% paraformaldehyde for 24 h at 4 °C, then embedded in OCT compound. These embedded tissues were quickly frozen in liquid nitrogen and stored at –80 °C until sectioned. Frozen blocks were sectioned at 15 μm thickness using a cryostat maintained at –27 °C. The sections were transferred onto poly-*L*-lysine-coated slides and kept at –20 °C until further processing. Subsequently, the sections were fixed in 4% paraformaldehyde for 10 min at room temperature. After fixation, sections were rinsed in tris buffered saline with Tween-20 (TBST)-Triton to remove any residual fixative. The sections were then blocked with a solution containing 5% normal goat serum and 0.3% Triton X-100 in tris buffered saline (TBS) for 1 h at room temperature. Overnight incubation with primary antibodies (IL-1β, IL-6, TNF-α, TLR4, p-NF-κB, NLRP3, ASC, caspase-1, GSDMD, ZO-1, occludin, claudin-1, and E-cadherin) was conducted at 4 °C in a humidified chamber, with antibody dilutions of 1:100 to 1:200 as per the manufacturer's instructions. Following primary antibody incubation, sections were washed three times in TBST-Triton for 5 min each. Fluorophore-conjugated secondary antibodies were then applied for 3 h at room temperature in darkness. After secondary antibody treatment, sections underwent three additional TBST-Triton washes. Nuclei staining was performed using 4′,6-diamidino-2-phenylindole dihydrochloride (DAPI)-containing antifade mounting medium for visualization. Imaging was executed on a confocal microscope

Table 2
Histological scoring criteria for colitis.

Infiltration of inflammatory cells	Goblet cell reduction	Degree of integrity of crypt structure	Score
Absence of infiltration	No damage	Normal morphology	0
The base of the crypt was infiltrated	Number of goblet cells was reduced	Crypt structure was slightly disrupted	1
Muscular mucosa was infiltrated	Number of goblet cells was greatly reduced	Crypt structure was extensively disrupted	2
Through the muscularis mucosa	The goblet cells were completely absent	Crypt structures disappeared	4

(Leica SP8) using consistent acquisition settings to maintain data uniformity, across the relevant excitation and emission spectra. Image quantification was carried out using the spot, surface, and colocalize functions in Imaris software, based on confocal microscopy image.

2.9 Quantitative real-time polymerase chain reaction (qPCR)

Colonic tissues were extracted from mice subsequent to their length measurements for the purpose of total RNA extraction. Initially, these tissues underwent homogenization, followed by treatment with specific reagents designed to isolate RNA. Once isolated, the RNA underwent reverse transcription to obtain cDNA. qPCR was then conducted in a thermal cycler, encompassing distinct cycles that included denaturation at 95 ℃ for 30 s, annealing at 53 ℃ for 60 s, and extension at 72 ℃ for 60 s. For the quantitative assessment, the gene expression of *IL-1β* (forward primer: 5′-TGCCACCTTTTGACAGTG ATG-3′, reverse primer: 5′-TGATGTGCTGCTGCGAGATT-3′), *IL-6* (forward primer: 5′-CCCCAATTTCCAATGCTCC-3′, reverse primer: 5′-CGCACTAGGTTTGCCGAGTA-3′), *TNF-α* (forward primer: 5′-GATCGGTCCCCAAAGGGATG-3′, reverse primer: 5′-CCACTTG GTGGTTTGTGAGTG-3′), *TLR4* (forward primer: 5′-GATCTGAGC TTCAACCCCCTG-3′, reverse primer: 5′-TCCACAGCCACCAGAT TCTC-3′), *NLRP3* (forward primer: 5′-AGATTACCCGCCCGAGAA AG-3′, reverse primer: 5′-TCCCAGCAAACCCATCCACT-3′), *ASC* (forward primer: 5′-GACAGTACCAGGCAGTTCGT-3′; reverse primer: 5′-AGTCCTTGCAGGTCAGGTTC-3′), *GSDMD* (forward primer: 5′-ATCCTGGCATTCCGAGTGG-3′; reverse primer: 5′-CTCT GGCCCACTGCTTTTCT-3′) were determined. These measurements were normalized against the expression of the housekeeping gene *GAPDH* (forward primer: 5′-TGAGGCCGGTGCTGAGTATGT-3′, reverse primer: 5′-CAGTCTTCTGGGTGGCAGTGAT-3′). The relative expression of the targeted genes was calculated using the $2^{-\Delta\Delta Ct}$ method.

2.10 Western blot

Colonic tissues were homogenized by lysis buffer with protease inhibitor cocktail. The homogenate was centrifuged (4 ℃, 12 000 × *g* for 10 min) to obtain supernatant. The supernatant was quantified by bicinchoninic acid (BCA) reagents and then mixed with loading buffer. Equal proteins were separated by sodium dodecyl sulfate-polyacrylamide gel electrophoresis. Proteins in the gel were then transferred onto a polyvinylidene difluoride membrane. The membrane was blocked with 5% bovine serum albumin (BSA) and then incubated with primary antibodies (1:1 000) followed by horseradish peroxidase-conjugated secondary antibody. The protein-antibody complex was finally detected using an enhanced chemiluminescence system. ImageJ software was used to quantify the grey value of the bands.

2.11 Transmission electron microscopy (TEM)

Colonic tissue samples were quickly fixed in 2.5% glutaraldehyde in 0.1 mol/L PBS for 2 h, and then thoroughly rinsed in 0.1 mol/L glycine to remove excess fixative. The tissues were embedded in epoxy resin, and initial sections of 1 mm^3 thickness were cut and stained with toluidine blue for 30 s, followed by a rinse in 0.1 mol/L PBS to eliminate any excess stain. For TEM analysis, ultra-thin sections around 60 nm thick were prepared from these samples. These sections were double-stained with uranyl acetate and lead citrate to enhance contrast. Under TEM, these stained sections provided detailed views of the cellular and subcellular structures.

2.12 Gut microbiota sequencing and analysis

After colon length measurement, fecal samples were collected and stored at –80 ℃ until microbiota analysis. Following 16S rRNA gene sequencing (338F: ACTCCTACGGGAGGCAGCAG; 806R: GGACTACHVGGGTWTCTAAT), sequences were refined, de-duplicated, and organized into operational taxonomic units (OTUs) based on 97% sequence similarity, the accepted criterion for bacterial species distinction. This clustering allows for the effective categorization and analysis of microbial taxa present in the samples. For each sample, bacterial community diversity was quantitatively assessed using *α*- and *β*-diversity indices. Additionally, hierarchical clustering analysis was then carried out to visually map the microbial community similarities and differences among the samples. Lastly, Spearman correlation analysis was performed to uncover potential relationships between gut microbiota and various factors of colitis, including symptoms, colonic inflammation, apoptosis, and intestinal barrier integrity.

2.13 Statistical analysis

Data are presented as the mean ± standard error of the mean. Normal distribution was firstly confirmed by Kolmogorov-Smirnov test. Group comparisons were made using a two-way ANOVA, and when significant differences were detected, Tukey's post hoc test was employed for pairwise comparisons. Differences were considered statistically significant when $P < 0.05$.

3. Results

3.1 Structural analysis of PSP

The microstructure of PSP was analyzed by SEM with a magnification of 500× and 5 000×. The image shows that PSP possesses a smooth, poreless surface and a dense composition predominantly of lamellar formations, adorned with numerous attached spherical entities (Figs. 1A and B).

FTIR revealed characteristic peaks indicative of functional groups in the polysaccharides (Fig. 1C). The broad absorption peak at 3 285.09 cm^{-1} corresponds to the –OH stretching vibrations, suggesting intramolecular or intermolecular hydrogen bonding in polysaccharides, with the broadening effect due to hydroxyl group formation. The peaks at 2 927.85 and 2 878.26 cm^{-1} are due to C–H bond stretching vibrations, typical of polysaccharides. The peak at 1 617.82 cm^{-1} is associated with the C=O stretching vibration of carbonyl groups. Additionally, the peaks at 1 151.30 and 1 080.87 cm^{-1} result from C–O–H stretching vibrations in the C–O–C bonds of the pyranose ring, indicating the presence of pyranose in the polysaccharide structure.

According to ^{1}H NMR (Fig. 1D), the results revealed distinct resonances at *δ* 2.51 and 3.35, attributed to DMSO and water, respectively. In the heteronuclear H1 region, spanning *δ* 4.3–6.0, predominant peak positions were observed at *δ* 5.10, 5.00, 4.91, and

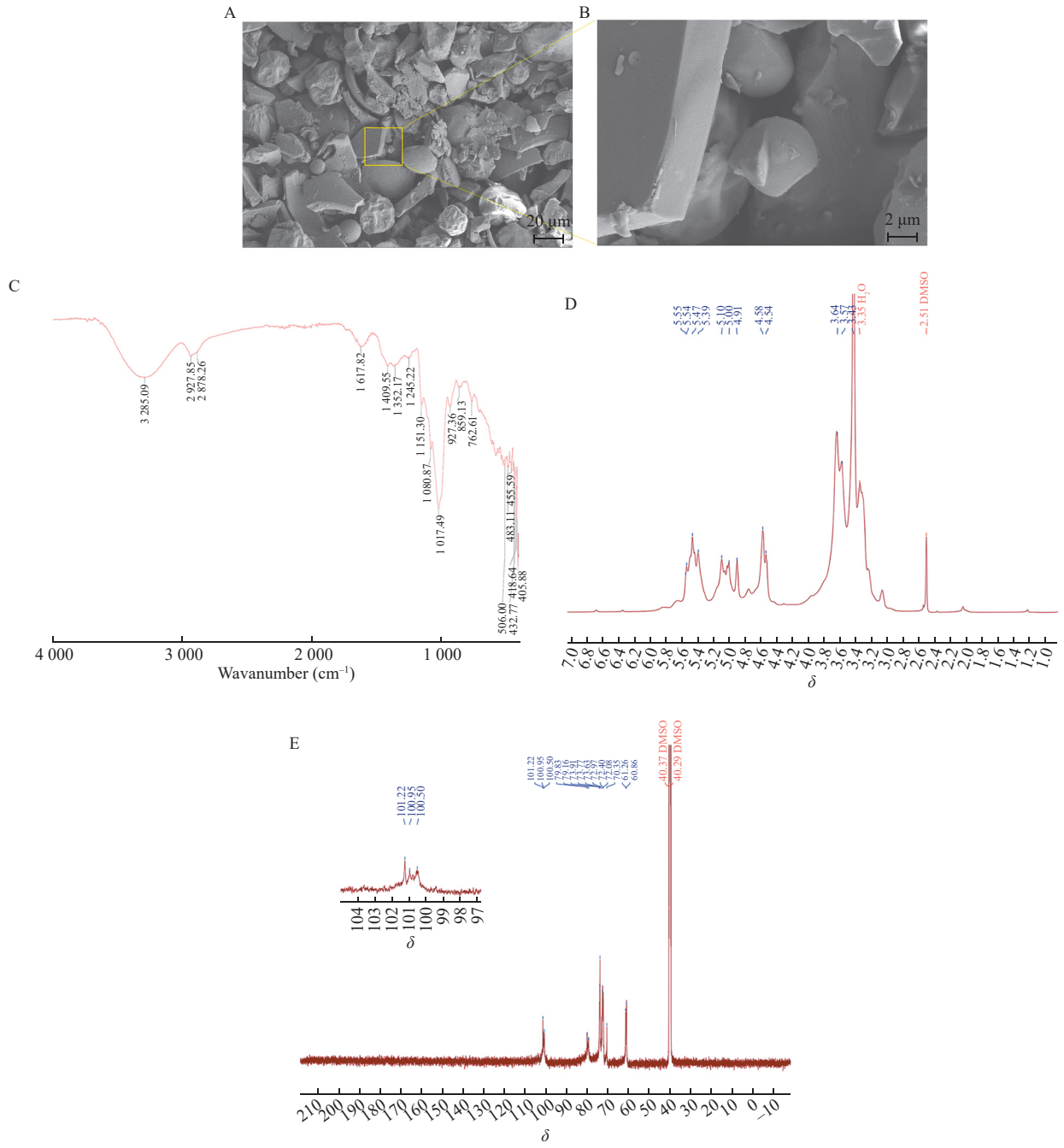


Fig. 1 Structural characterization and morphology of PSP isolated from *P. sibiricum*. (A) SEM picture with a magnification of 500×; (B) SEM picture with a magnification of 5 000×. (C) FT-IR spectra; (D) ^{1}H NMR spectra; (E) ^{13}C NMR spectra.

4.58. These peaks corroborate the presence of a diverse array of residues within the polysaccharide, further indicating the coexistence of both α- and β-configuration residues, with α-configurations being more prominent. The interval between δ 3.0–4.0 in the proton spectrum exhibited typical signals outside the heteroatoms of the residue rings, characterized by hydroxyl and alkyl protons. The heterogeneity of signals in this region aligns with the typical spectral characteristics of polysaccharides, denoting a complex structure.

According to ^{13}C NMR (Fig. 1E), no significant carbon signals of glyoxalate carbonyls were found within δ 170–210, confirming that the polysaccharide is neutral. Within the δ 90–110 heterohead region of the carbon spectrum, three principal heterohead carbon signals were identified at δ 101.22, 100.95, and 100.50. These signals, corresponding to the heterohead carbon C1, resonated with multiple heterohydrogen H1 signals, confirming the presence of abundant residual sugars in the polysaccharide. Signals within the δ 55–85 range highlighted multiple typical polysaccharide residual sugar peaks, notably at δ 60.86 and 61.26, which are likely attributed to the methylene-CH_2-secondary carbons, indicative of pyranose C_6 or furanose C_5 structures. Furthermore, the presence of multiple signals between δ 70–75 provided additional insights into the carbon framework of the residual sugars, identifying carbons located at the C2–C5 positions for pyranose and C2–C4 for furanose residues.

3.2 PSP ameliorated colitis symptoms in DSS-induced mice

As shown in Fig. 2, there was a significant reduction in DAI following PSP administration, highlighting its effectiveness in reducing colitis severity. Additionally, a substantial decrease in diarrhea frequency was noted, further affirming the beneficial role on gastrointestinal symptoms commonly associated with colitis. Moreover, an increase in colon length was observed in DSS-treated animals receiving PSP, suggesting its therapeutic efficacy. Together, these results emphasize the potential of PSP as a treatment for colitis, meriting further investigation into its mechanisms of action.

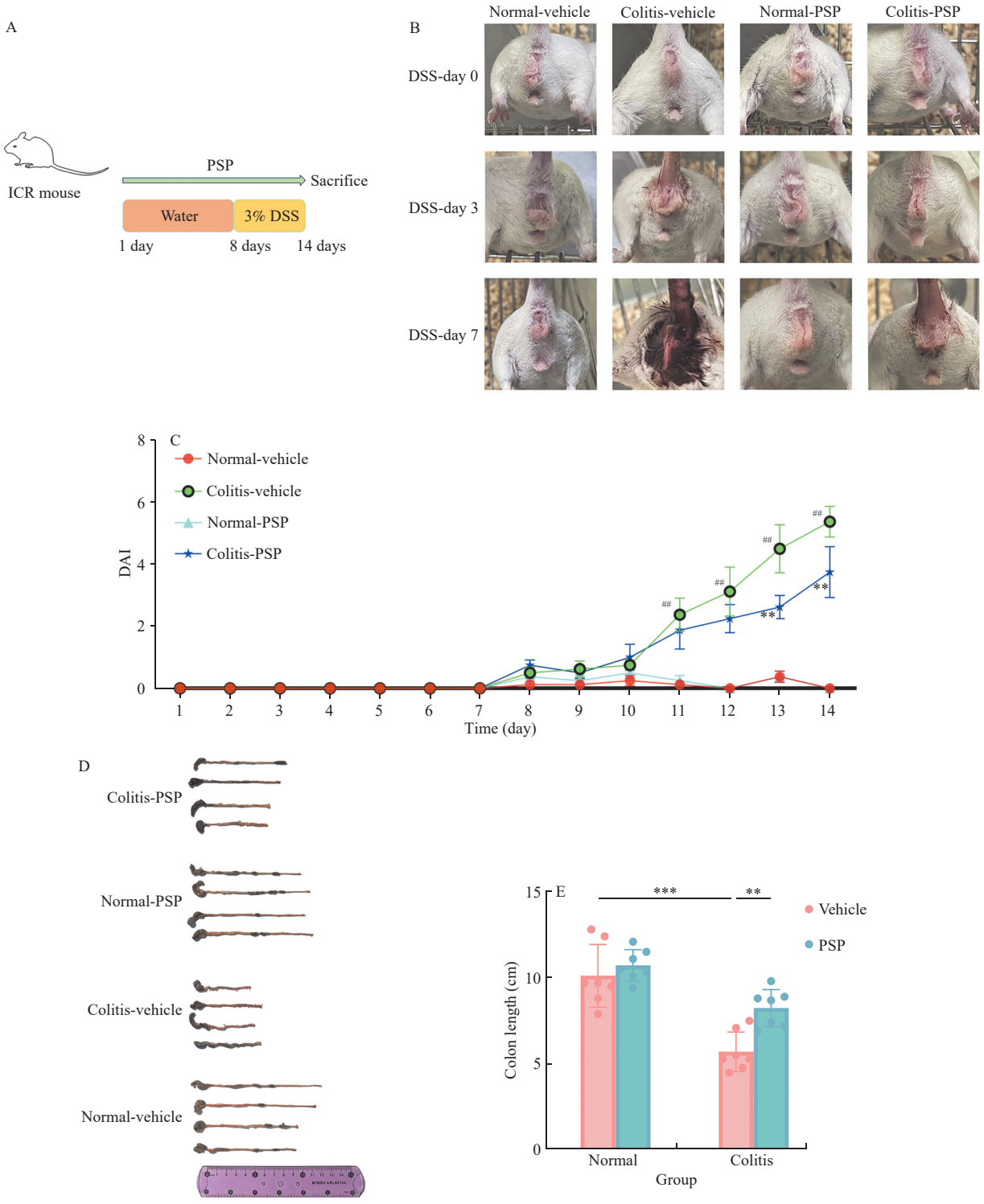


Fig. 2 Administration with PSP attenuated DSS-induced colitis in mice. (A) Schematic illustration of the procedure for the experiment. (B) Representative diarrhea in each group. (C) DAI scores of mice throughout the experiment. (D) Representative colon anatomy of mice in each group. (E) Colon length. Data are presented as mean ± standard error of the mean ($n = 7$). $^{**}P < 0.01$, $^{***}P < 0.001$.

3.3 PSP reversed DSS-induced colitis histopathological change

As shown in Figs. 3A and B, in normal animals, in terms of morphology, the colonic crypts exhibit a tubular and orderly arrangement, and appear to be evenly spaced and extend uniformly from the mucosal surface to the muscularis mucosa. The epithelial lining looks intact with no disruptions or erosions. The cells exhibit regular columnar morphology, and goblet cells, which produce mucus, are interspersed regularly. The lamina propria, which fills the space between the crypts, appears to have a normal amount of connective tissue without evident edema or excessive fibrosis. In terms of infiltrated immune cells, there are not a prominent infiltration of neutrophils. A few scattered lymphocytes can be seen in the lamina propria and eosinophils are present in minimal numbers but aren't overtly evident. In DSS-induced colitis mice, the glands appear disrupted in some areas, indicating damage to the crypt architecture. The lamina propria, the connective tissue layer, appears densely populated with cells, indicating an inflammatory reaction. In terms of infiltrated immune cells, there are multiple areas in the image that show an infiltration of polymorphonuclear leukocytes (neutrophils), which are indicative of an acute inflammatory reaction. There also appears to be an increased number of mononuclear cells, such as lymphocytes and plasma cells, in the lamina propria, suggesting a chronic component to the inflammation. Besides, areas of epithelial loss and erosion would be indicative of ulcerations, a feature commonly seen in colitis. However, after the administration with PSP, the colonic glands appear more preserved and organized compared to the typical disrupted appearance seen in DSS-induced colitis. The crypts are largely well-ordered and tubular. The epithelial lining of the crypts seems largely intact with minimal evidence of epithelial cell damage or erosion. The lamina propria shows less cellular infiltration compared to a severe colitis scenario, suggesting a reduction in inflammation. In terms of infiltrated immune cells, there are fewer areas showing infiltration of neutrophils, suggesting a reduction in acute inflammation. Although there is still evidence of some mononuclear cell infiltration in the lamina propria, it appears reduced compared to untreated colitis. There's a marked reduction in typical pathological features of DSS-induced colitis such as cryptitis, abscesses, and ulceration, suggesting PSP exhibit promising therapeutic effects against DSS-induced colitis, at least based on this histological evaluation.

As shown in Figs. 3C and D, in normal animals, the distribution of the PAS-positive staining appears to be even, suggesting a normal distribution of goblet cells within the colonic tissue. There are no areas of overt depletion or over-concentration of goblet cells. The number and distribution of goblet cells appear within normal limits, suggesting that mucin production and secretion are functioning properly. In DSS-induced colitis mice, the number of goblet cells is reduced in several crypts compared to normal colonic tissue. This reduction can be a feature of colitis, as goblet cell loss is common in inflammatory conditions. The mucin pool appears depleted in certain areas of the tissue. In comparison to the colitis mice, it is evident that PSP treatment has resulted in the preservation of goblet cell and the restoration of mucin content within goblet cells.

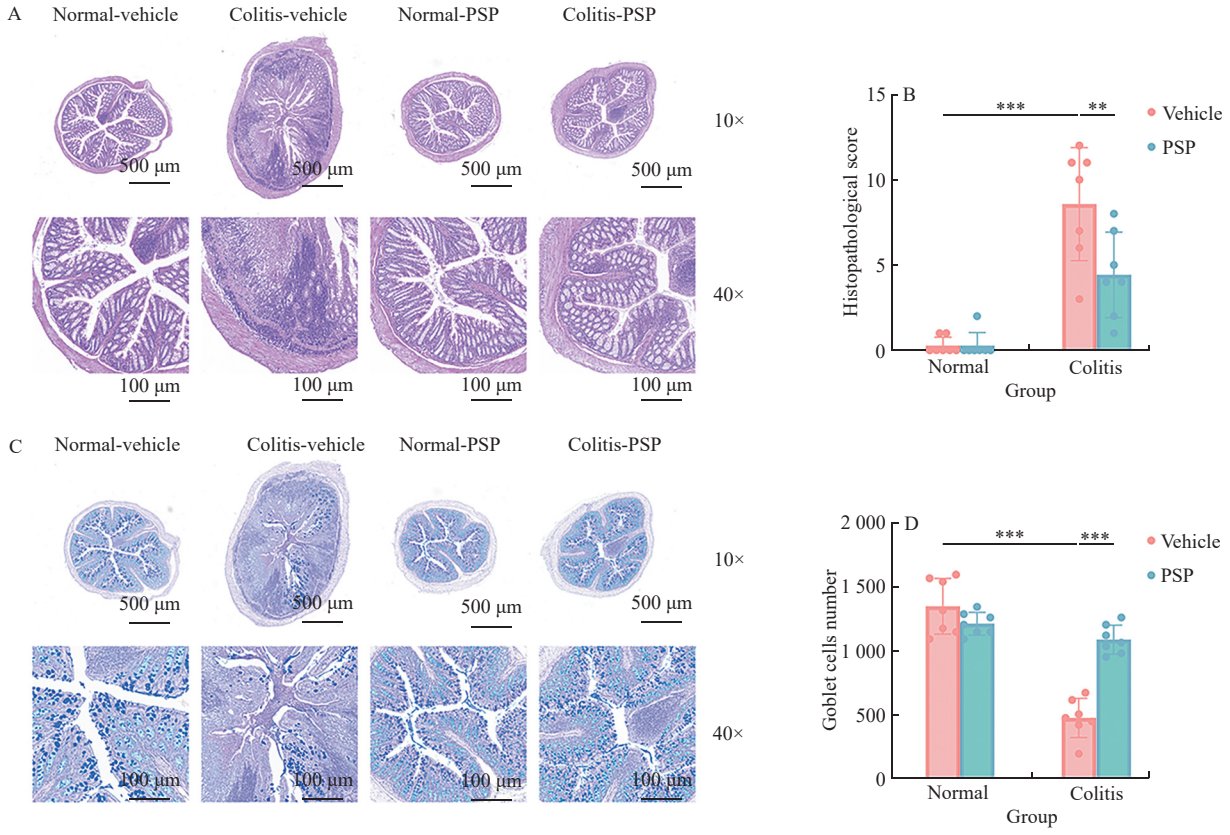


Fig. 3 Histopathological changes and scores of colonic tissues of mice in each group after the treatment with PSP. (A) Representative H&E staining histopathological image of each group (10× and 40×). (B) Histopathological score. (C) Representative PAS staining image of each group (10× and 40×). (D) Goblet cells number. Data are presented as mean ± standard error of the mean ($n = 7$). $^{**}P < 0.01$,$^{***}P < 0.001$.

3.4 PSP inactivated colonic pro-inflammatory phenotype macrophage

Immunofluorescence of colonic tissue slices showed that DSS induced macrophage ($CD68^+$) in the colon (Figs. 4A and B). Moreover, DSS increased the number (Fig. 4C) and the proportions (Fig. 4D) of pro-inflammatory ($CD68^+iNOS^+$) phenotype macrophage. PSP partially reversed these changes in the colon of DSS mice. These results suggest that PSP switches the phenotype of activated macrophage from pro-inflammatory to anti-inflammatory, which may be involved in the colonic protection of PSP.

Fig. 5 demonstrates the strong anti-inflammatory effect of PSP in DSS-induced mice models of colitis. Cytokines such as IL-1β, IL-6, and TNF-α, known to drive the inflammatory response in colonic lesions, were significantly elevated in the colitis mice but were markedly reduced following PSP treatment (Figs. 5A–C). The study further explored the mechanism behind this anti-inflammatory activity, finding that the reduction in cytokine levels was largely due to the suppression of the TLR4/NF-κB signaling pathway. This pathway plays a crucial role in inflammation, and its inhibition by PSP accounts for the decreased cytokine levels. The activation of TLR4/NF-κB signaling by DSS was notably curtailed by PSP (Figs. 5D and E). Additionally, qPCR analysis corroborated the immunofluorescence findings, showing that the mRNA levels of these cytokines, elevated by DSS, were suppressed following PSP treatment (Figs. 5F–H). However, the expression of *TLR4* in colonic tissues remained unchanged by either DSS or PSP treatment (Fig. 5I).

3.5 PSP alleviated NLRP3/ASC/Caspase-1/GSDMD mediated pyroptosis in DSS-induced colitis mice

In further experiments, we focused on the potential of PSP to inhibit the NLRP3/ASC/Caspase-1/GSDMD-mediated pyroptosis signaling pathway in the colon. Immunofluorescence results showed that DSS exposure significantly increased the protein levels of NLRP3, ASC, caspase-1, and GSDMD-N, key components of the pyroptotic pathway (Figs. 6A–H). Notably, PSP treatment led to a substantial reduction in the levels of these proteins. qPCR results confirmed that the gene expression of *NLRP3*, *ASC*, and *GSDMD* was significantly upregulated by DSS, whereas PSP effectively reduced the expression of *NLRP3* and *ASC* (Figs. 6I–K). Moreover, Western blot indicated that PSP significantly decreased the protein levels of NLRP3, caspase-1, and GSDMD-N in DSS-induced colitis (Figs. 6L–P). These findings suggest that PSP has the capacity to partially inhibit the NLRP3/ASC/Caspase-1/GSDMD-mediated pyroptosis signaling pathway in colitis.

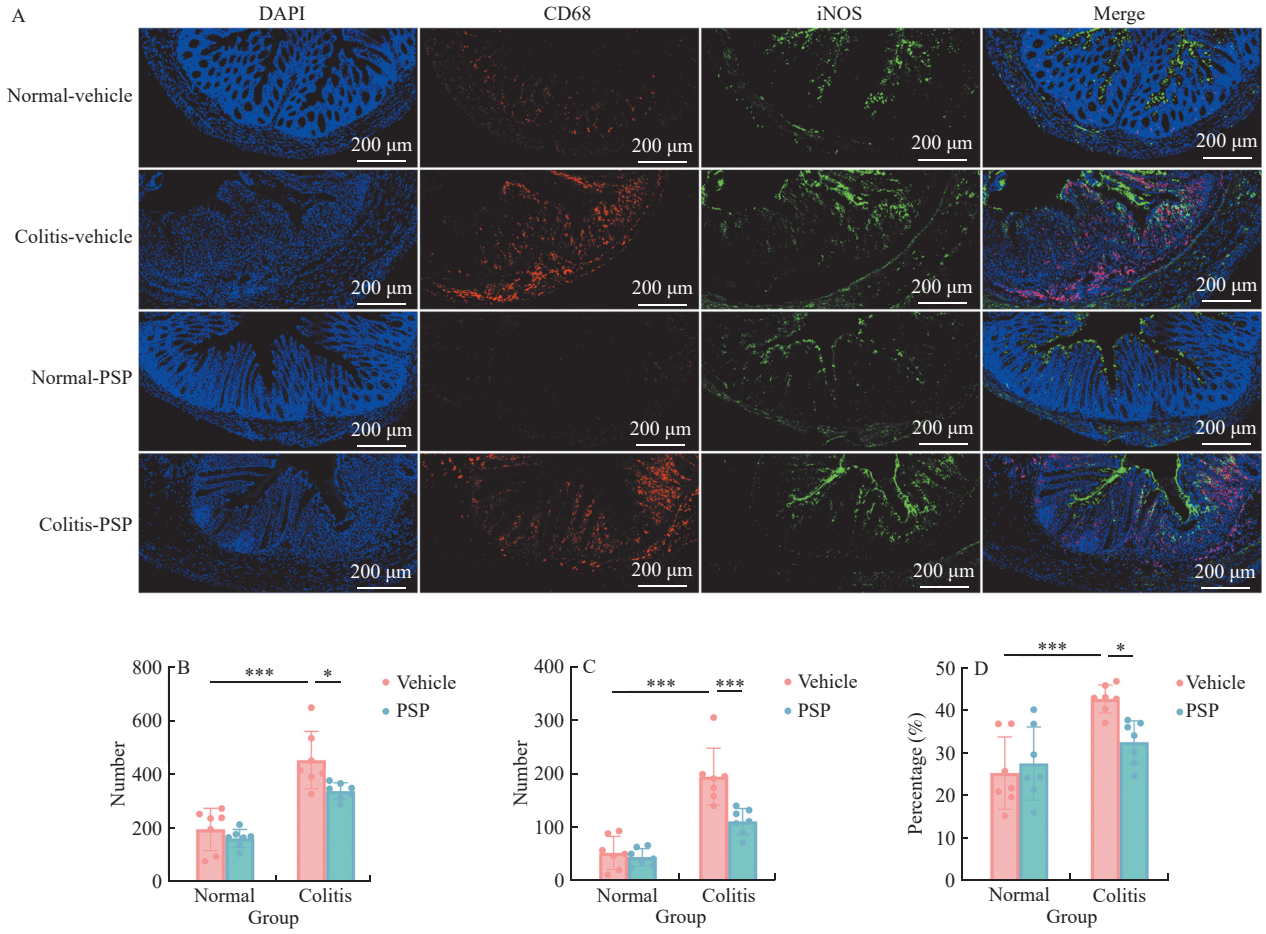


Fig. 4 PSP decreased colonic CD68 labeled macrophage in DSS-induced colitis mice. (A) Representative immunofluorescence image of each group. CD68 were labelled with red at 568 nm, iNOS was labelled with green at 488 nm, and nucleus was labelled by DAPI at 405 nm. The image magnification is 100×, and scale bar was set as 200 μm. (B) Number of $CD68^+$ macrophage. (C) Number of $CD68^+iNOS^+$ M1 macrophage. (D) Percentage of M1 macrophage to macrophage. Data are presented as mean ± standard error of the mean ($n = 7$). *$P < 0.05$, ***$P < 0.001$.

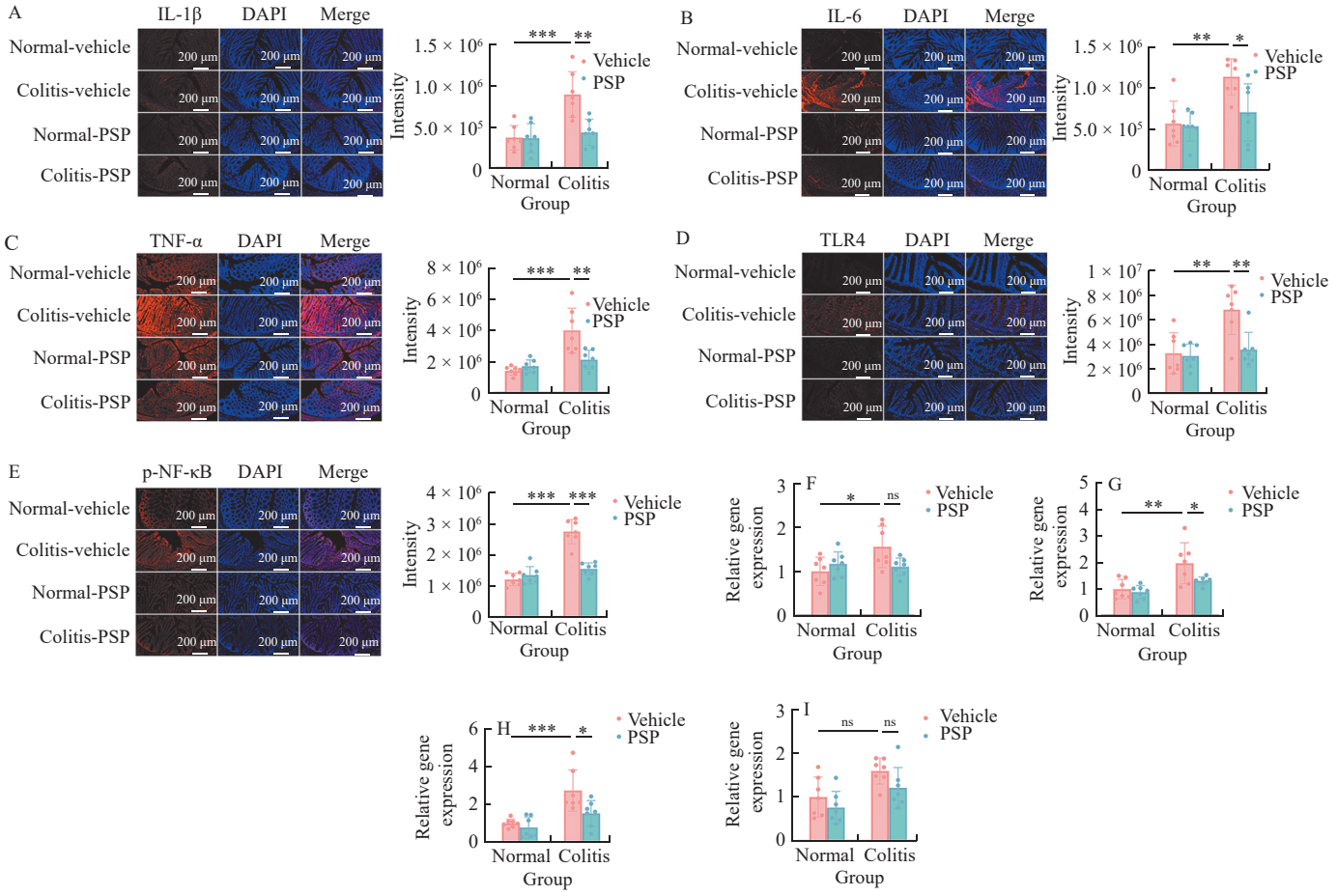


Fig. 5 PSP alleviated colonic inflammation in DSS-induced colitis mice. (A) IL-1β, (B) IL-6, (C) TNF-α, (D) TLR4 and (E) p-NF-κB levels detected by immunofluorescence. The proteins were labelled with red at 488 nm, and nucleus was labelled by DAPI at 405 nm. The image magnification is 100×, and scale bar was set as 200 μm. The mRNA expression of cytokines including (F) *IL-1β*, (G) *IL-6*, (H) *TNF-α* and (N) *TLR4*. Data are presented as mean ± standard error of the mean ($n = 7$). $^{*}P < 0.05$, $^{**}P < 0.01$, $^{***}P < 0.001$, ns indicates no significance.

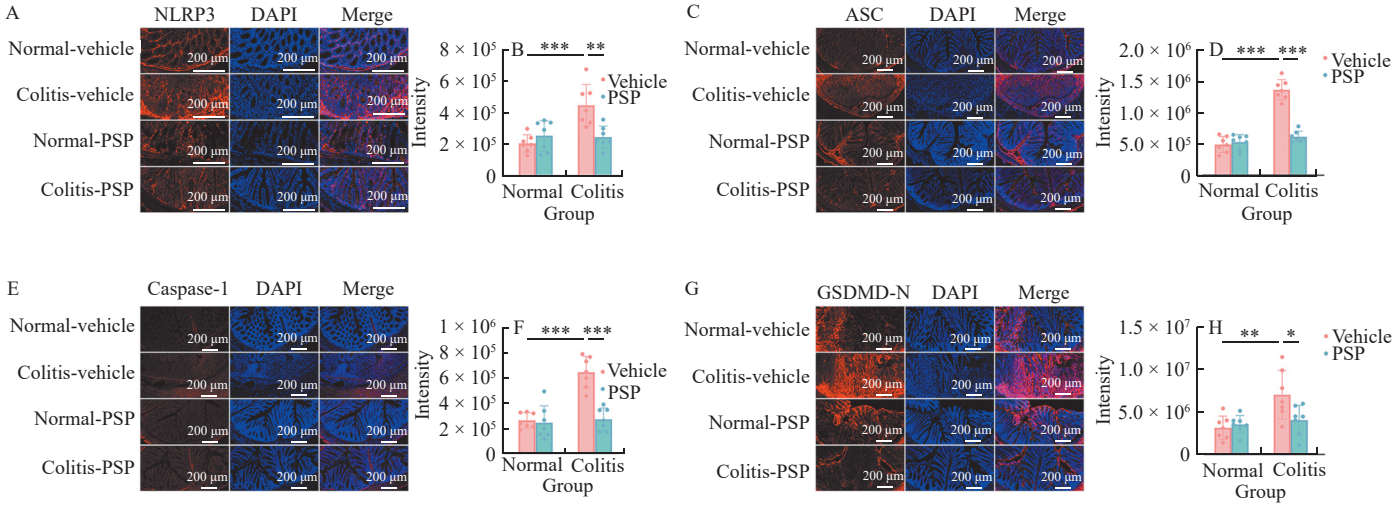


Fig. 6 PSP attenuated colonic NLRP3/ASC/Caspase-1/GSDMD mediated pyroptosis in DSS-induced colitis mice. (A, B) NLRP3, (C, D) ASC, (E, F) Caspase-1, and (G, H) GSDMD-N levels detected by immunofluorescence. The proteins were labelled with red at 488 nm, and nucleus was labelled by DAPI at 405 nm. The image magnification is 100×, and scale bar was set as 200 μm. The mRNA expression of (I) *NLRP3*, (J) *ASC*, and (K) *GSDMD*. Western blot image (L) and protein levels of (M) NLRP3, (N) ASC, (O) Caspase-1, and (P) GSDMD-N. Data are presented as mean ± standard error of the mean ($n = 7$). $^{*}P < 0.05$, $^{**}P < 0.01$, $^{***}P < 0.001$, ns indicates no significance.

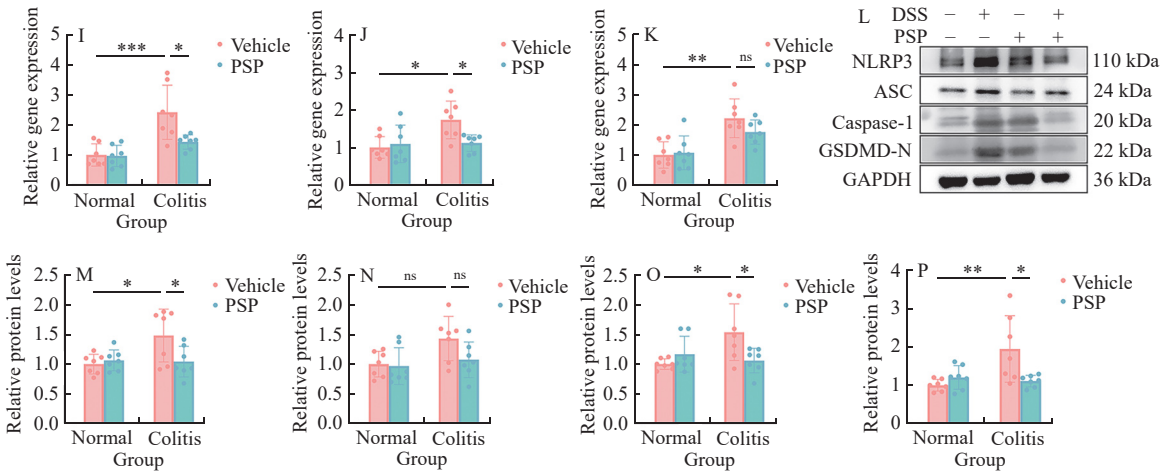


Fig. 6 (*Continued*)

3.6 PSP reversed the ultrastructural mitochondria damages during pyroptosis in DSS-induced colitis mice

Pyroptosis, an inflammatory form of programmed cell death, is characterized by pore formation on cell membranes, release of cellular contents, and activation of inflammatory responses. Mitochondria play a crucial role in pyroptosis process, with GSDMD-N not only instigating mitochondrial damage during pyroptosis but also severely disrupting both inner and outer mitochondrial membranes. Such damage leads to mitochondrial dysfunction, including hypoplasia[16]. In this way, we employed TEM to examine the ultrastructural cellular damage in colitis, focusing on mitochondrial integrity (Fig. 7). In the colitis-vehicle group, a significant reduction in mitochondrial count was noted, along with an increase in damaged mitochondria compared to the normal-vehicle group. Conversely, pretreatment with PSP substantially ameliorated these mitochondria alterations, in both quantity and condition. This indicates the ability of PSP to protect against GSDMD-N-induced pyroptosis in colitis by maintaining mitochondrial integrity and functionality.

3.7 PSP enhanced the intestinal barrier by increasing ZO-1, occludin, claudin-1, and E-cadherin expression

In a further elucidation of the therapeutic effects of PSP, as presented in Fig. 8, our study examined the impact of DSS and PSP

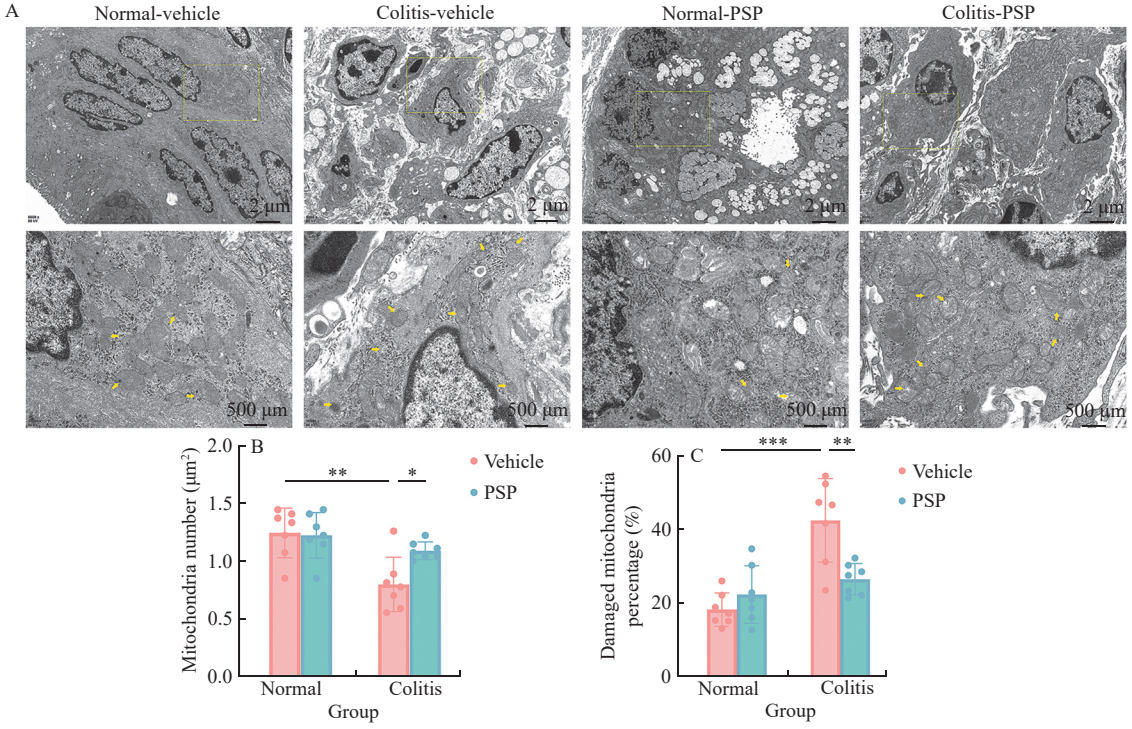


Fig. 7 The ultrastructural damages of colonic tissue in DSS-induced colitis mice. (A) Representative images of the cell morphology and mitochondria of each group, the yellow arrow indicate damaged mitochondria. The image magnification is 8 000× and 30 000×, respectively. The scale bar was set as 2 μm and 500 nm, respectively. (B) Mitochondria number. (C) Damaged mitochondria percentage. Data are presented as mean ± standard error of the mean ($n = 7$). *$P < 0.05$, **$P < 0.01$, ***$P < 0.001$.

on the integrity of the intestinal barrier, which plays a crucial role in maintaining gastrointestinal homeostasis and function. DSS led to significant impairment of the intestinal barrier, prominently signified by a decrease in the expression of tight junction proteins. Tight junctions are crucial components of the intestinal barrier, acting as gatekeepers that regulate the paracellular transport and maintain epithelial polarity. On the contrary, PSP treatment appeared to markedly enhance the integrity of this barrier. This was evidenced through the upregulation of key tight junction and adherens junction proteins, including ZO-1, occludin, claudin-1, and E-cadherin. These proteins are integral to the structural and functional fortitude of the intestinal barrier, each playing distinct but synergistic roles. ZO-1 contributes to the structural composition of tight junctions, while occludin and claudin-1 are central in the formation of tight junction strands that control paracellular permeability. E-cadherin, pivotal in the adherens junctions, further consolidates cell-cell adhesion and barrier integrity.

However, both immunofluorescence and Western blot indicated that PSP significantly restored barrier integrity, demonstrated by the increased levels of ZO-1, claudin-1, and E-cadherin. On the other hand, immunofluorescence instead of Western blot showed that occludin levels were decreased in colitis and increased after PSP administration. This difference might be mainly attributed to the different sample collecting positions. Our sampling procedure began at the distal end of the colon, and four 0.5 cm pieces of colon were sequentially sampled for H&E/PAS staining, immunofluorescence, PCR and Western blot. Therefore, the tissue samples used for immunofluorescence were obtained from the distal colon near the anus, and that area is where the colitis firstly occurred. Besides, previous research indicated that mice with compromised epithelial barrier function exhibited reduced levels of ZO-1 and claudin-8, while occludin levels remained unchanged[17]. This suggests that occludin may be less sensitive to detect disruptions than other barrier proteins.

3.8 PSP reshaped gut microbiota compositions in DSS-induced colitis

In our investigation, we evaluated the impact of PSP administration on the gut microbiota compositions in colitis mice. Firstly, *α*-diversity index indicated that there was a significant reduction of ACE index of OTU level in colitis mice as compared with normal mice, while PSP could increase the ACE index (Fig. 9A). Principal coordinates analysis (PCoA), an analysis of *β*-diversity index, was also used to discern the variations in microbial community structure. Consistently, PCoA revealed a marked divergence in the gut microbiota composition between colitis-induced mice and normal mice. Notably, PSP treatment appeared to reshape the gut microbiota composition of the colitis mice closer to that of the normal mice, a significant change observable at both phylum and genus levels (Figs. 9B and C). At the phylum level, Bacteroidota and Firmicutes emerged as the predominant groups in the gut microbiota. In terms of phyhum level, Bacteroidota, Firmicutes and Proteobacteria were identified as the three most abundant phyla (Fig. 9D). Subsequent detailed analysis revealed a significant decrease in the relative abundance of Bacteroidota, whereas a significant increase in the relative abundance of Proteobacteria in the colitis group (Fig. 9E). Further exploration at the genus level indicated notable alterations in the gut microbiota due to colitis (Fig. 9F). Specifically, the relative abundance of g_unclassified_f_Muribaculaceae, *Lactobacillus*, Clostridia_UCG-014, and Lachnospiraceae_NK4A136_group was decreased in the colitis group. Conversely, the relative abundance of *Enterobacter*, *Escherichia-Shigella*, and *Blautia* exhibited an increase in the colitis mice (Fig. 9G). In contrast, administration of PSP demonstrated a capacity to reverse these alterations.

Linear discriminant analysis effect size (LEfSe) was employed to assess the compositional differences in intestinal microbiota among the

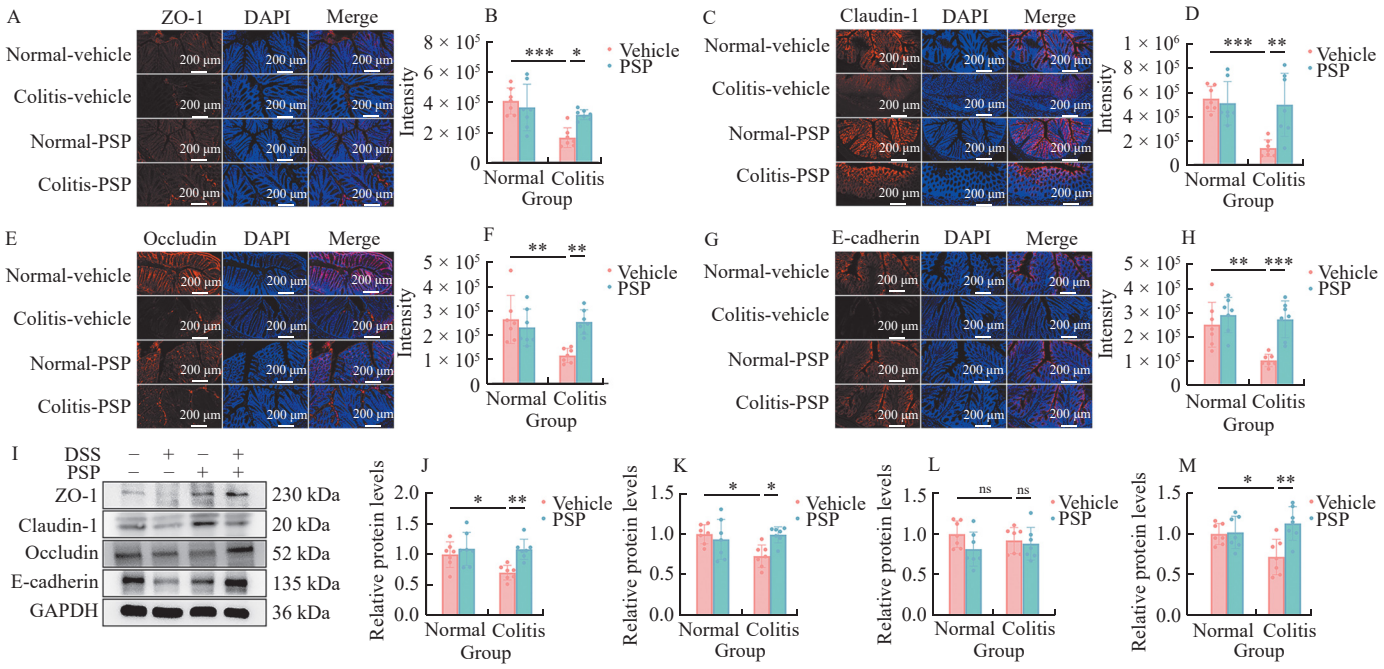


Fig. 8 PSP increased intestinal barrier proteins in DSS-induced colitis mice. (A, B) ZO-1, (C, D) claudin-1, (E, F) occludin, and (G, H) E-cadherin detected by immunofluorescence. The proteins were labelled with red at 488 nm, and nucleus was labelled by DAPI at 405 nm. The image magnification is 100×, and scale bar was set as 200 μm. Western blot image (I) and protein levels of (J) ZO-1, (K) claudin-1, (L) occludin, and (M) E-cadherin. Data are presented as mean ± standard error of the mean ($n = 7$). *$P < 0.05$, **$P < 0.01$, ***$P < 0.001$, ns indicates no significance.

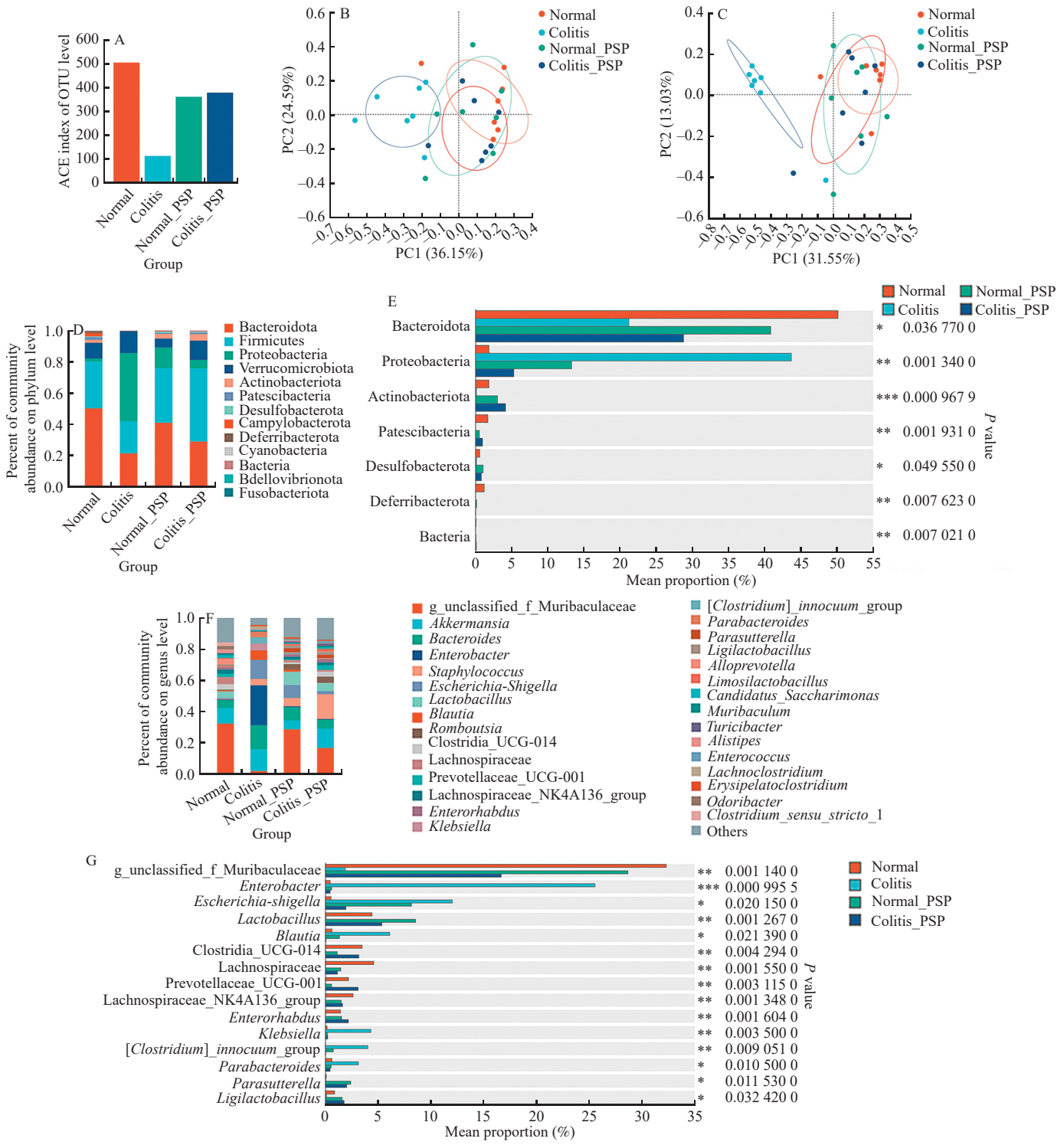


Fig. 9 PSP increased the relative abundance of gut microbiota in DSS-induced colitis mice. (A) ACE index of α-diversity by one-way ANOVA. (B) PCoA diagram of gut microbiota at phylum level. (C) PCoA diagram of gut microbiota at genus level. (D) Percentage of relative abundance of gut microbiota at phylum level. (E) Differential gut microbiota at phylum levels. (F) Percentage of relative abundance of gut microbiota at genus level. (G) Differential gut microbiota at genus levels. Data are presented as mean ($n = 7$). *$P < 0.05$, **$P < 0.01$, ***$P < 0.001$.

tested groups and to identify the dominant microbiota within each group. As shown in Fig. 10, a comparison between the colitis and normal mice groups revealed significant differences. Specifically, there was a notable increase in the abundance of bacteria from the phylum Proteobacteria and genus *Enterobacter* and *Escherichia-Shigella* in the colitis group, whereas normal mice exhibited a higher abundance of bacteria from the phylum Bacteroidota and genus unclassified_f_Muribaculaceae. Following treatment with PSP, the dominant bacteria in the colitis group were identified as belonging to the phylum Actinobacteriota and genus Prevotellaceae_UCG-001. Besides, Fig. 10 provides a comprehensive overview of the distribution of other bacterial taxa among the four groups.

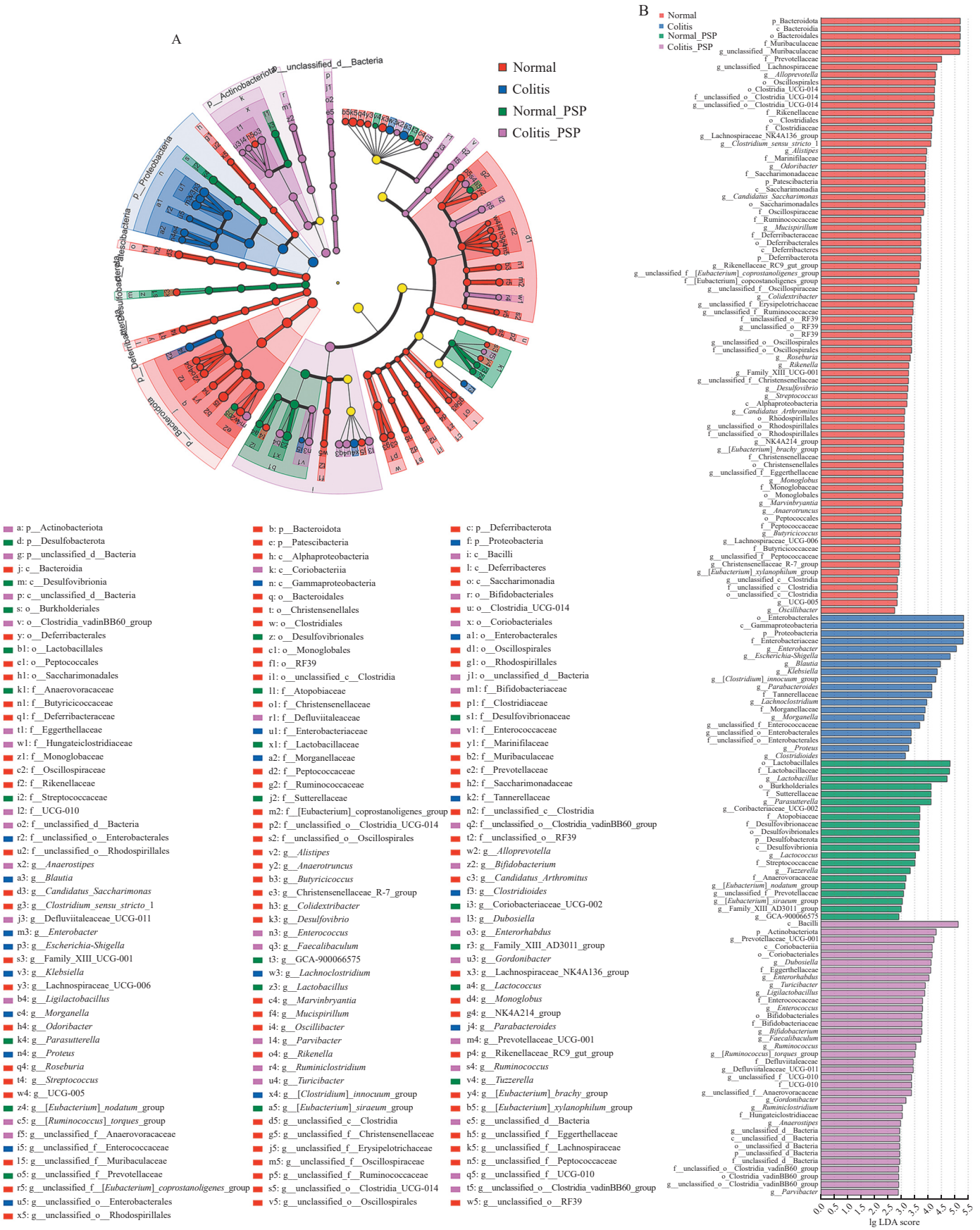


Fig. 10 Species differentiation and specific species under the effects of PSP. (A) LEfSe analysis histogram and (B) LDA score. Data are presented as mean (n = 7).

Overall, these observations indicated that PSP not only normalized the altered relative abundance of the aforementioned phylum and genus but also overall reshaped the gut microbiota composition in the DSS-induced colitis model.

3.9 Correlation analysis between gut microbiota and serum pro-inflammatory cytokines and stress hormone

To further delineate the associations between gut microbiota alterations and various aspects of colitis pathology, including colitis symptoms, colonic inflammation, pyroptosis, and tight junction protein expression, a comprehensive Spearman correlation analysis was conducted in response to PSP administration. At the phylum level, as demonstrated in Fig. 11, our analysis revealed a notable correlation between Patescibacteria and all measured parameters in this study, indicating a broad-spectrum association of this phylum with colitis-related changes. Additionally, the phylum Proteobacteria displayed significant correlations with nearly all assessed parameters, with the exception of colonic TLR4 levels, suggesting its potential involvement in colitis pathophysiology and the treatment of PSP. Expanding our analysis to the genus level, as shown in Fig. 12, we observed that certain genus specifically *Enterobacter*, Lachnospiraceae, *Odoribacter*, and *Candidatus_Saccharimonas*, exhibited correlations with all evaluated parameters. This suggests a widespread influence of these genus on the therapeutical effects of PSP.

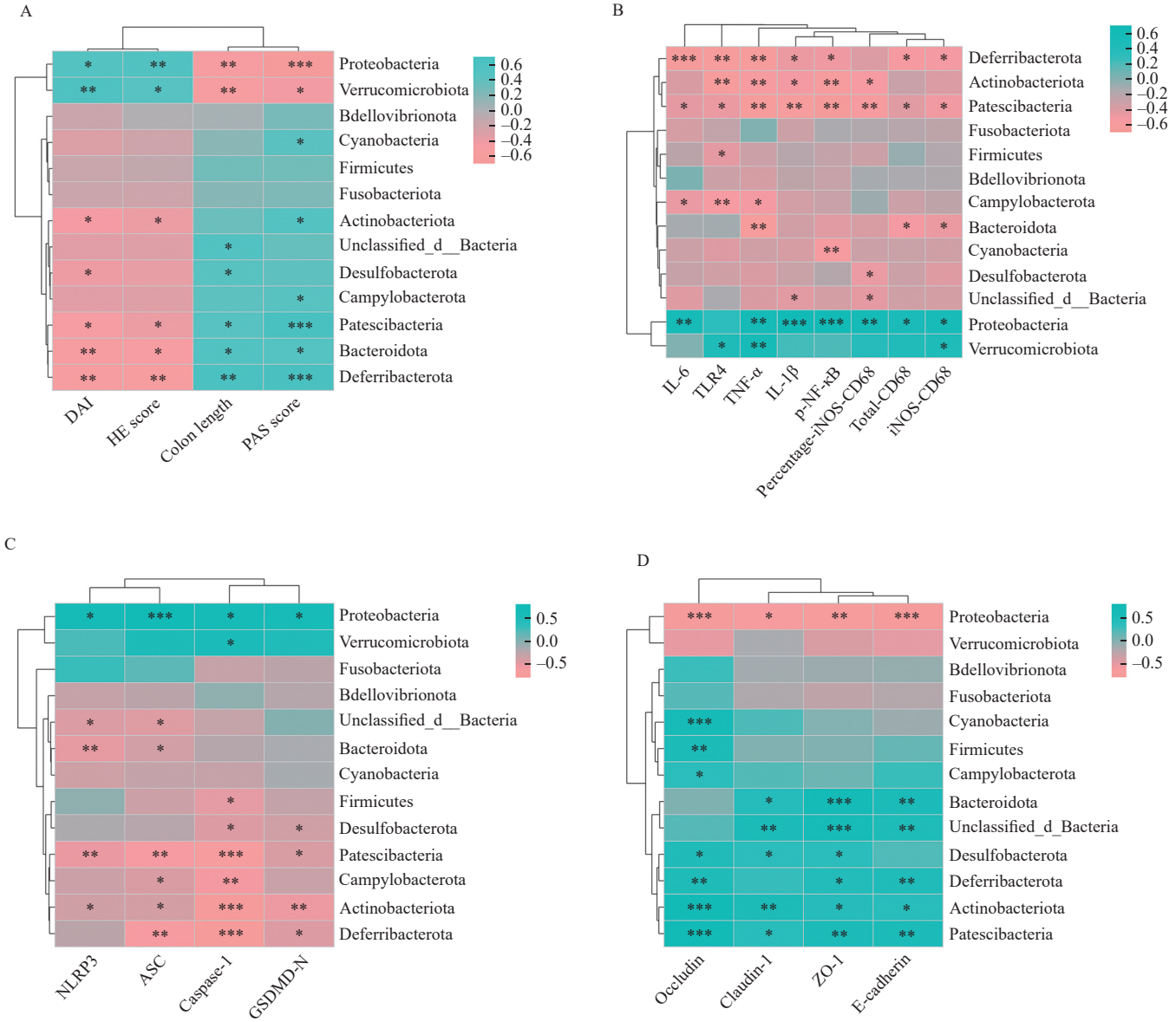


Fig. 11 Spearman correlation heatmap post-PSP administration at phylum level. (A) The correlations between gut microbiota and markers of colonic inflammation. (B) The correlation matrix between gut microbiota and the mRNA expression of inflammation related genes. (C) The association between gut microbiota and colonic NLRP3/ASC/Caspase-1/GSDMD proteins. (D) The correlation between gut microbiota and the expression of colonic tight junction proteins. $n = 7$ per group. $^{*}P < 0.05$, $^{**}P < 0.01$, $^{***}P < 0.001$.

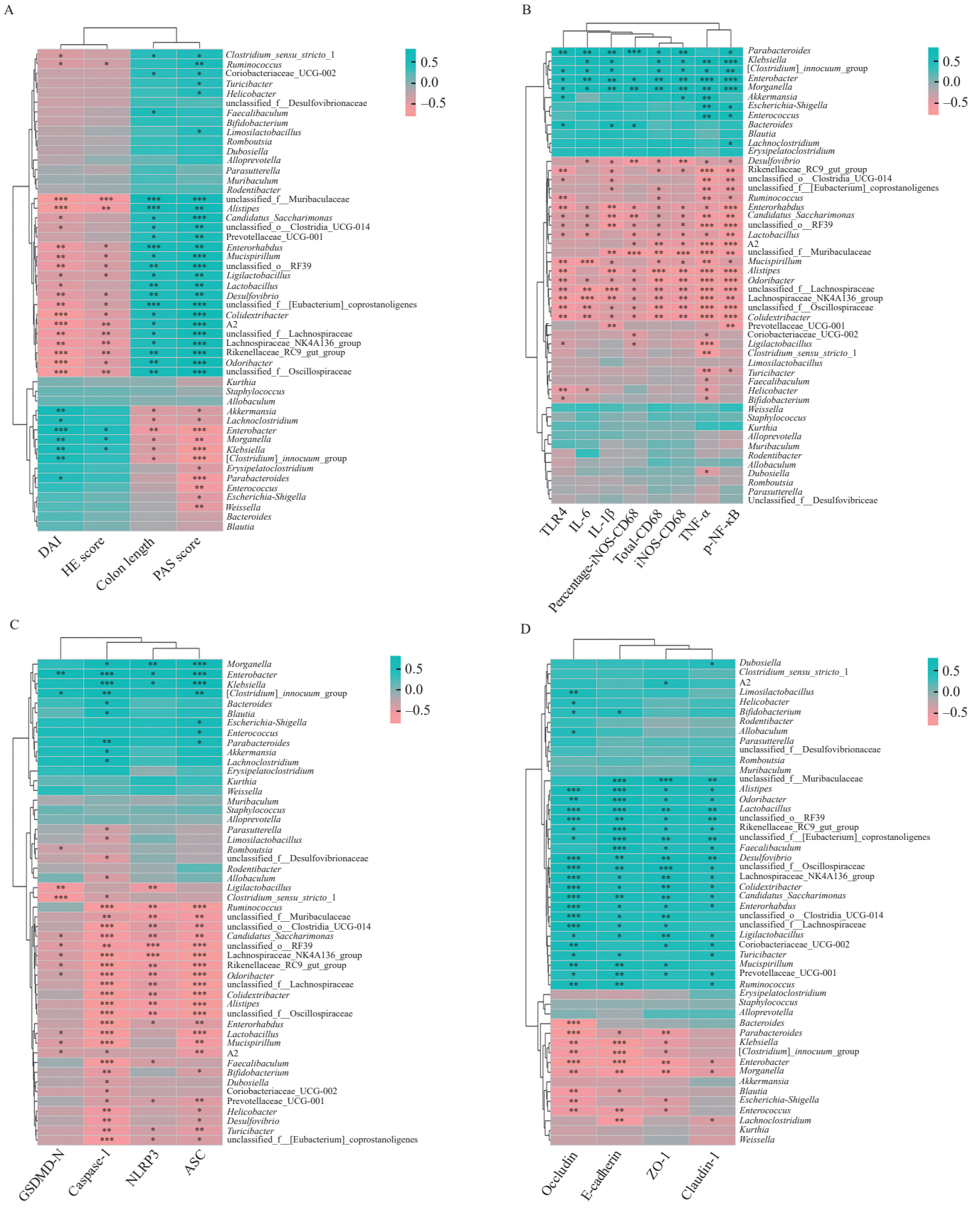


Fig. 12 Spearman correlation heatmap post-PSP administration at genus level. (A) The correlations between gut microbiota and markers of colonic inflammation. (B) The correlation matrix between gut microbiota and the mRNA expression of inflammation related genes. (C) The association between gut microbiota and colonic NLRP3/ASC/Caspase-1/GSDMD proteins. (D) The correlation between gut microbiota and the expression of colonic tight junction proteins. $^{*}P < 0.05$, $^{**}P < 0.01$, $^{***}P < 0.001$.

4. Discussion

P. sibiricum, traditionally recognized for its health benefits, has shown promise in modulating inflammatory responses[8]. However, its impact on inflammatory responses in colitis has been unexplored. This research not only extracted and characterized the polysaccharides from *P. sibiricum* but also elucidated the potential mechanism of PSP in alleviating colitis for the first time (Fig. 13). This finding is significant, presenting a natural alternative to synthetic drugs for colitis management.

The TLR4/NF-κB signaling pathway plays a critical role in the pathogenesis of colitis[18]. TLR4 acts as a pattern recognition receptor that identifies microbial imbalances and triggers immune responses upon detecting pathogen-associated molecular patterns. Activation of this receptor leads to the activation of the NF-κB pathway, which is pivotal in regulating the transcription of inflammatory genes. In colitis, increased TLR4 activation intensifies the inflammatory process, resulting in elevated levels of pro-inflammatory cytokines like IL-1β, IL-6, and TNF-α[19]. Continuous NF-κB activation sustains the chronic inflammation in the intestine, exacerbating the cycle of mucosal injury and immune response. The TLR4/NF-κB pathway is essential in colitis pathophysiology[20-21]. In the present study, our results demonstrated that PSP could suppress this pathway, thereby reducing the cytokines IL-1β, IL-6, and TNF-α and diminishing the inflammatory response. This finding underscores the effectiveness of *P. sibiricum* in influencing key inflammatory pathways and emphasizes its therapeutic potential.

Within the complex cellular processes underlying colitis pathophysiology, pyroptosis stands out as a vital type of inflammatory cell death, marked by cell swelling, plasma membrane permeabilization, and the release of pro-inflammatory cellular contents[22]. Governed by the NLRP3/ASC/Caspase-1/GSDMD signaling pathway, pyroptosis involves the activation of the NLRP3 inflammasome, which recruits and interacts with ASC, subsequently activating caspase-1. Activated caspase-1 cleaves GSDMD, whose N-terminal fragment forms membrane pores, causing cell swelling, membrane rupture, and the discharge of inflammatory cytokines and cell contents, leading to pyroptosis[23-24]. In the current investigation, we observed significant modulation of pyroptotic markers (NLRP3 inflammasome, ASC, caspase-1, and GSDMD-N) in colonic tissues post-PSP treatment, indicating that PSP's effects are mediated through the modulation of pyroptotic signaling pathways. Additionally, a key feature of pyroptosis is mitochondrial damage and depletion, which precedes cell lysis and inflammatory content release[4]. TEM analysis revealed considerable improvement in mitochondrial abnormalities with PSP treatment, suggesting a lowered pyroptotic activity. Since mitochondrial dysfunction is an early indicator of pyroptosis[16]. Therefore, our results imply that the therapeutic benefits of PSP extend beyond modulating pyroptotic signaling pathways to also include preservation of mitochondrial integrity in colonic cells, thus offering protection against pyroptotic damage.

The gastrointestinal tract is essential for nutrient absorption and acts as an important barrier against external harmful entities. The core of this barrier function is the intestinal epithelium, which is a single cell layer bound by complex protein structures that regulate its permeability. Tight junctions, primarily comprising ZO-1, occludin, and claudin-1, are essential in this context. They form multiprotein complexes that preserve the selective permeability of the paracellular space, allowing nutrient uptake while blocking pathogens and toxins[25]. ZO-1, a peripheral membrane protein, collaborates with membrane proteins like occludin and claudins to create this barrier[26]. Occludin, known for its regulatory role in tight junction permeability, contributes to barrier integrity and function[27], while claudin-1, a prominent claudin family member, is integral to the paracellular barrier selectivity[28]. Meanwhile, E-cadherin strengthens the epithelial layer by facilitating cell adhesion[29]. In colitis, an inflamed colon condition, the intestinal barrier is often compromised, contributing to and resulting from disease progression[30]. Alterations in ZO-1, occludin, claudin-1, and E-cadherin levels can lead to a "leaky" intestinal barrier, enabling the uncontrolled entry of bacteria, toxins, and antigens. This disruption can intensify the inflammatory response, aggravate colitis pathology[31-33]. Hence, repairing the

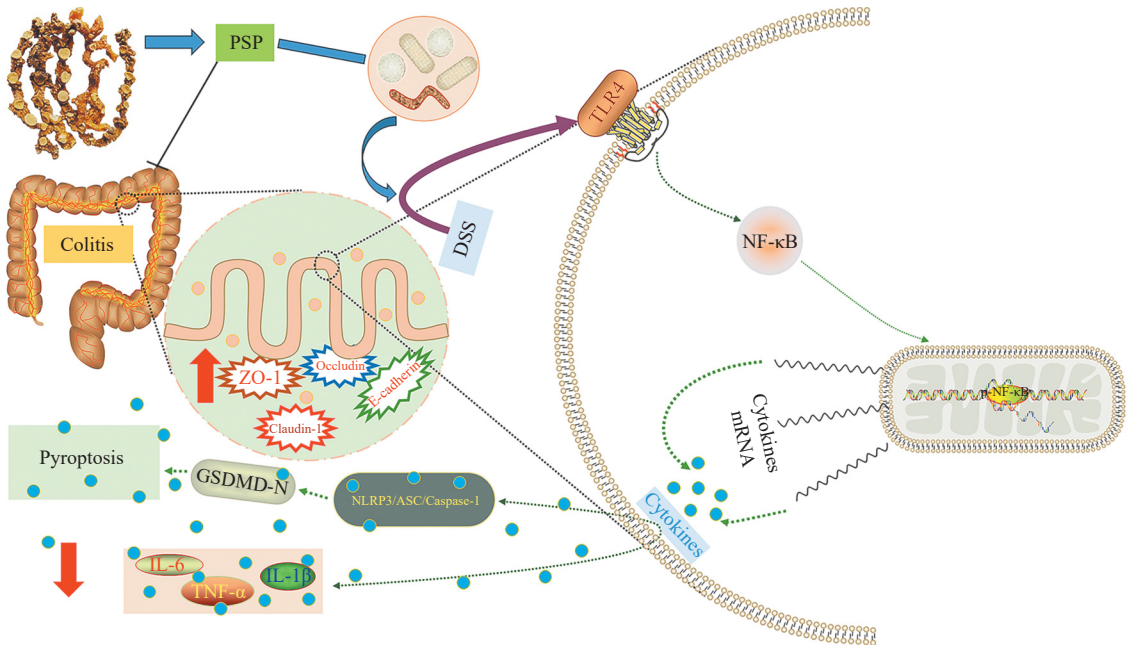


Fig. 13 Mechanical diagram of PSP for the pyroptosis regulation of colonic cells in colitis.

intestinal mucosal barrier is essential for attenuating colitis, highlighting the role of PSP in not only reducing inflammation but also in restoring the gut mucosa's structural and functional integrity.

Colitis is closely associated with alterations in the gut microbiota, where dysbiosis, characterized by an imbalance between beneficial and harmful bacterial species, can exacerbate the inflammatory processes inherent to the disease[34-35]. The composition and diversity of the gut microbiota are crucial in colitis pathogenesis, affecting both immune responses and intestinal barrier integrity[36-37]. In the current study, the results showed that DSS decreased the abundance of Bacteroidota, which typically contributes to the maintenance of gut health through the production of short-chain fatty acids[38]. Thus, Bacteroidota is crucial for colonocyte health and anti-inflammatory responses. A decline in Bacteroidota may thus impair colonic health and immune functionality[39]. On the other hand, an increase in Proteobacteria, often linked to gut dysbiosis, correlates with heightened inflammation. This phylum includes pathogenic bacteria that can aggravate gut inflammation and compromise the mucosal barrier[40]. The reduction in genus such as g_unclassified_f_Muribaculaceae, *Lactobacillus*, Clostridia_UCG-014, and Lachnospiraceae_NK4A136_group, which are keys to gut barrier maintenance and anti-inflammatory processes, indicates a deteriorated gut environment typical of colitis[41-42]. The rise in *Enterobacter*, *Escherichia-Shigella*, and *Blautia* within the colitis suggests a shift towards harmful bacteria, potentially aggravating the disease. The ability of PSP to normalize these genus underscores its potential in rebalancing the gut microbiota, thus alleviating colitis symptoms. Spearman correlation analysis further elucidates the interaction between gut microbiota and PSP administration, revealing a comprehensive correlation of the phylum Patescibacteria and genus *Enterobacter*, Lachnospiraceae_NK4A136_group, *Odoribacter*, and *Candidatus_Saccharimonas* with all measured biomarkers. The ability of PSP to restore the balance of these critical gut microbiota suggests its potential in modulating the gut environment, possibly by promoting the growth of beneficial bacteria or by inhibiting pathogenic or pro-inflammatory microbes. This modulation of the microbiota composition by PSP may contribute to reducing colonic inflammation and enhancing gut barrier functionality.

In comparison to other natural and synthetic compounds targeting the TLR4/NF-κB and NLRP3/ASC/Caspase-1/GSDMD pathways, PSP demonstrates a unique dual-action mechanism. For instance, mesalamine, a commonly used synthetic compound for colitis, primarily reduces inflammation but lacks the broader impacts on gut microbiota and barrier function that PSP exhibits. Curcumin, another natural compound, has been noted for its anti-inflammatory effects via NF-κB inhibition but may not have the same extensive gut microbiota modulation as PSP. Therefore, PSP stands out for its multifunctional approach, addressing inflammation, pyroptosis, and microbiota composition, which suggests its potential as a comprehensive treatment option for colitis.

5. Conclusion

This study isolated a lamellar-structured polysaccharide from *P. sibiricum*, exploring its physicochemical and structural characteristics, along with its anti-colitis efficacy. The findings confirmed the hypothesis that PSP can attenuate colitis through its anti-inflammatory properties. Additionally, the study revealed that the effectiveness of PSP may be attributed to the suppression of the NLRP3/ASC/Caspase-1/GSDMD-mediated pyroptosis signaling pathway and the modulation of the gut microbiota. The present findings provide a foundation for future investigations into the dietary applications of PSP and their incorporation into comprehensive colitis management strategies. Moreover, these insights pave the way for additional studies on the role of PSP in chronic gastrointestinal diseases, indicating a possible shift towards bioactive compounds in dietary interventions for colitis and similar conditions, and thus fostering innovative, natural therapeutic strategies.

Conflict of interest

The authors declare that there is no conflict of interest.

Acknowledgements

This work was supported by Xiamen Science and Technology Plan Project (3502Z20226034), Xiamen Marine and Fishery Development Special Fund (23YYZP013QCA11) and Natural Science Foundation of Fujian Province (2022J01315). We would like to thank Instrumental Analysis Center of Huaqiao University for the help of confocal testing, and thank Dr. Xiao-Hua Guo for the help of NMR testing.

References

[1] B. Khor, A. Gardet, R.J. Xavier, Genetics and pathogenesis of inflammatory bowel disease, Nature 474 (2011) 307-317. https://doi.org/10.1038/nature10209.

[2] A.N. Ananthakrishnan, C.N. Bernstein, D. Iliopoulos, et al., Environmental triggers in IBD: a review of progress and evidence, Nat. Rev. Gastroenterol. Hepatol. 15 (2018) 39-49. https://doi.org/10.1038/nrgastro.2017.136.

[3] M.L. Hoivik, B. Moum, I.C. Solberg, et al., Work disability in inflammatory bowel disease patients 10 years after disease onset: results from the IBSEN Study, Gut 62 (2013) 368-375. https://doi.org/10.1136/gutjnl-2012-302311.

[4] S. Zhang, Y. Liang, J. Yao, et al., Role of pyroptosis in inflammatory bowel disease (IBD): from gasdermins to DAMPs, Front. Pharmacol. 13 (2022) 833588. https://doi.org/10.3389/fphar.2022.833588.

[5] X. Chen, G. Liu, Y. Yuan, et al., NEK7 interacts with NLRP3 to modulate the pyroptosis in inflammatory bowel disease via NF-κB signaling, Cell Death Dis. 10 (2019) 906. https://doi.org/10.1038/s41419-019-2157-1.

[6] R. Miao, C. Jiang, W.Y. Chang, et al., Gasdermin D permeabilization of mitochondrial inner and outer membranes accelerates and enhances pyroptosis, Immunity 56(11) (2023) 2523-2541. https://doi.org/10.1016/j.immuni.2023.10.004.

[7] X. Pan, Q. Zhu, L.L. Pan, et al., Macrophage immunometabolism in inflammatory bowel diseases: from pathogenesis to therapy, Pharmacol. Ther. 238 (2022) 108176. https://doi.org/10.1016/j.pharmthera.2022.108176.

[8] X. Cui, S. Wang, H. Cao, et al., A review: the bioactivities and pharmacological applications of *Polygonatum sibiricum* polysaccharides, Molecules 23 (2018) 1170. https://doi.org/10.3390/molecules23051170.

[9] P. Zhao, C. Zhao, X. Li, et al., The genus *Polygonatum*: a review of ethnopharmacology, phytochemistry and pharmacology, J. Ethnopharmacol. 214 (2018) 274-291. https://doi.org/10.1016/j.jep.2017.12.006.

[10] X. Zhu, Q. Li, F. Lu, et al., Antiatherosclerotic potential of *Rhizoma Polygonati* polysaccharide in hyperlipidemia-induced atherosclerotic hamsters, Drug Res. 65 (2015) 479-483. https://doi.org/10.1055/s-0034-1387756.

[11] D. Liu, W. Tang, C. Han, et al., Advances in *Polygonatum sibiricum* polysaccharides: extraction, purification, structure, biosynthesis, and bioactivity, Front. Nutr. 9 (2022) 1074671. https://doi.org/10.3389/fnut.2022.1074671.

[12] J. Su, Y. Wang, M. Yan, et al., The beneficial effects of *Polygonatum sibiricum* Red. superfine powder on metabolic hypertensive rats via gut-derived LPS/TLR4 pathway inhibition, Phytomedicine 106 (2022) 154404. https://doi.org/10.1016/j.phymed.2022.154404.

[13] Y. Zhang, Y. Sun, Y. Liu, et al., *Polygonum sibiricum* polysaccharides exert the antidepressant-like effects in chronic unpredictable mild stress-induced depressive mice by modulating microbiota-gut-brain axis, Phytother. Res. 37 (2023) 3408-3423. https://doi.org/10.1002/ptr.7813.

[14] W. Zhou, J. Hong, T. Liu, et al., *Polygonatum* polysaccharide regulates macrophage polarization and improves LPS-induced acute lung injury through TLR4-MAPK/NF-κB pathway, Can. Respir. J. 2022 (2022) 2686992. https://doi.org/10.1155/2022/2686992.

[15] Z. Liu, S. Fayyaz, D. Zhao, et al., *Polygonatum sibiricum* polysaccharides improve cognitive function in *D*-galactose-induced aging mice by regulating the microbiota-gut-brain axis, J. Funct. Foods 103 (2023) 105476. https://doi.org/10.1016/j.jff.2023.105476.

[16] L. Zhang, Y.F. Tang, P. Huang, et al., Role of NLRP3 inflammasome in central nervous system diseases, Cell Biosci. 14 (2024) 75. https://doi.org/10.1186/s13578-024-01256-y.

[17] M. Basic, M. Buettner, L.M. Keubler, et al., Loss of CD14 leads to disturbed epithelial-B cell crosstalk and impairment of the intestinal barrier after *E. coli* Nissle monoassociation, Sci. Rep. 8 (2018) 719. https://doi.org/10.1038/s41598-017-19062-7.

[18] D. Impellizzeri, R. Fusco, T. Genovese, et al., *Coriolus versicolor* downregulates TLR4/NF-κB signaling cascade in dinitrobenzenesulfonic acid-treated mice: a possible mechanism for the anti-colitis effect, Antioxidants 11 (2022) 406. https://doi.org/10.3390/antiox11020406.

[19] M.F. Neurath, Cytokines in inflammatory bowel disease, Nat. Rev. Immunol. 14 (2014) 329-342. https://doi.org/10.1038/nri3661.

[20] S.H. Lee, J.E. Kwon, M.L. Cho, Immunological pathogenesis of inflammatory bowel disease, Intest. Res. 16 (2018) 26-42. https://doi.org/10.5217/ir.2018.16.1.26.

[21] N. Mikuda, R. Schmidt-Ullrich, E. Kargel, et al., Deficiency in IκBα in the intestinal epithelium leads to spontaneous inflammation and mediates apoptosis in the gut, J. Pathol. 251 (2020) 160-174. https://doi.org/10.1002/path.5437.

[22] J.V. Patankar, C. Becker, Cell death in the gut epithelium and implications for chronic inflammation, Nat. Rev. Gastroenterol. Hepatol. 17 (2020) 543-556. https://doi.org/10.1038/s41575-020-0326-4.

[23] Z. Liu, C. Wang, J. Yang, et al., Caspase-1 engages full-length gasdermin D through two distinct interfaces that mediate caspase recruitment and substrate cleavage, Immunity 53 (2020) 106-114.e105. https://doi.org/10.1016/j.immuni.2020.06.007.

[24] S. Xia, Z. Zhang, V.G. Magupalli, et al., Gasdermin D pore structure reveals preferential release of mature interleukin-1, Nature 593 (2021) 607-611. https://doi.org/10.1038/s41586-021-03478-3.

[25] N. Roehlen, A.A. Roca Suarez, H. El Saghire, et al., Tight junction proteins and the biology of hepatobiliary disease, Int. J. Mol. Sci. 21 (2020) 825. https://doi.org/10.3390/ijms21030825.

[26] S. Sun, J. Zhou, Phase separation as a therapeutic target in tight junction-associated human diseases, Acta Pharmacol. Sin. 41 (2020) 1310-1313. https://doi.org/10.1038/s41401-020-0470-y.

[27] C. Chelakkot, J. Ghim, S.H. Ryu, Mechanisms regulating intestinal barrier integrity and its pathological implications, Exp. Mol. Med. 50 (2018) 1-9. https://doi.org/10.1038/s12276-018-0126-x.

[28] S. Cuzic, M. Antolic, A. Ognjenovic, et al., Claudins: beyond tight junctions in human ibd and murine models, Front. Pharmacol. 12 (2021) 682614. https://doi.org/10.3389/fphar.2021.682614.

[29] H. Yuksel, M. Ocalan, O. Yilmaz, E-Cadherin: an important functional molecule at respiratory barrier between defence and dysfunction, Front. Physiol. 12 (2021) 720227. https://doi.org/10.3389/fphys.2021.720227.

[30] G. Rogler, A. Singh, A. Kavanaugh, et al., Extraintestinal manifestations of inflammatory bowel disease: current concepts, treatment, and implications for disease management, Gastroenterology 161 (2021) 1118-1132. https://doi.org/10.1053/j.gastro.2021.07.042.

[31] S. Yu, Y. Sun, X. Shao, et al., Leaky gut in IBD: intestinal barrier-gut microbiota interaction, J. Microbiol. Biotechnol. 32 (2022) 825-834. https://doi.org/10.4014/jmb.2203.03022.

[32] H. Usuda, T. Okamoto, K. Wada, Leaky gut: effect of dietary fiber and fats on microbiome and intestinal barrier, Int. J. Mol. Sci. 22 (2021) 7613. https://doi.org/10.3390/ijms22147613.

[33] N. Tajik, M. Frech, O. Schulz, et al., Targeting zonulin and intestinal epithelial barrier function to prevent onset of arthritis, Nat. Commun. 11 (2020) 1995. https://doi.org/10.1038/s41467-020-15831-7.

[34] S.L. Wang, M.M. Zhang, H. Zhou, et al., Inhibition of NLRP3 attenuates sodium dextran sulfate-induced inflammatory bowel disease through gut microbiota regulation, Biomed. J. 46 (2023) 100580. https://doi.org/10.1016/j.bj.2023.01.004.

[35] J. Li, Y. Ji, N. Chen, et al., Colitis-associated carcinogenesis: crosstalk between tumors, immune cells and gut microbiota, Cell Biosci. 13 (2023) 194. https://doi.org/10.1186/s13578-023-01139-8.

[36] L. Wang, M. Li, Y. Gu, et al., Dietary flavonoids-microbiota crosstalk in intestinal inflammation and carcinogenesis, J. Nutr. Biochem. 125 (2023) 109494. https://doi.org/10.1016/j.jnutbio.2023.109494.

[37] D. Li, J. Zhou, L. Wang, et al., Gut microbial metabolite deoxycholic acid facilitates Th17 differentiation through modulating cholesterol biosynthesis and participates in high-fat diet-associated colonic inflammation, Cell Biosci. 13 (2023) 186. https://doi.org/10.1186/s13578-023-01109-0

[38] H. Zafar, M.H. Saier, Jr., Gut *Bacteroides* species in health and disease, Gut Microbes 13 (2021) 1-20. https://doi.org/10.1080/19490976.2020.1848158.

[39] Y. Zhou, F. Zhi, Lower level of *Bacteroides* in the gut microbiota is associated with inflammatory bowel disease: a meta-analysis, Biomed. Res. Int. 2016 (2016) 5828959. https://doi.org/10.1155/2016/5828959.

[40] G. Rizzatti, L.R. Lopetuso, G. Gibiino, et al., Proteobacteria: a common factor in human diseases, Biomed. Res. Int. 2017 (2017) 9351507. https://doi.org/10.1155/2017/9351507.

[41] X. Shao, C. Sun, X. Tang, et al., Anti-inflammatory and intestinal microbiota modulation properties of Jinxiang garlic (*Allium sativum* L.) polysaccharides toward dextran sodium sulfate-induced colitis, J. Agric. Food. Chem. 68 (2020) 12295-12309. https://doi.org/10.1021/acs.jafc.0c04773.

[42] X. Huang, J. Hu, H. Zhang, et al., *Clostridium butyricum* and chitooligosaccharides in synbiotic combination ameliorate symptoms in a DSS-induced ulcerative colitis mouse model by modulating gut microbiota and enhancing intestinal barrier function, Microbiol. Spectr. 11 (2023) e0437022. https://doi.org/10.1128/spectrum.04370-22.